MSDE

PAPER

View Article Online
View Journal | View Issue

Cite this: *Mol. Syst. Des. Eng.*, 2024, **9**, 856

Boron subphthalocyanine axial groups: a comprehensive set for studying the tuning of photophysical and electrochemical properties†

Rachel Zigelstein [a] and Timothy P. Bender *[abcd]

Eighteen boron subphthalocyanines (BsubPcs) axial derivatives were synthesized through axial exchange reactions with Br-BsubPc under relatively mild conditions to systematically study the influence of a structurally diverse array of axial group derivatives on the physical properties of the BsubPcs. The photophysical and electrochemical properties of BsubPcs were investigated through solution-state UV-vis absorbance and fluorescence spectroscopy, relative fluorescence quantum yield (QY), cyclic voltammetry (CV), and differential pulse voltammetry (DPV), as these properties are crucial for the application of BsubPcs in the field of organic electronics. The impact of the axial groups on photophysical properties was evaluated by taking measurements in both toluene and α,α,α-trifluorotoluene as the solvent, and referencing QY to two compounds. The axial group has a minimal impact on the absorbance and fluorescence peak shifts, with α,α,α-trifluorotoluene causing a slight blueshift. The axial group had a significant impact on QY, with values ranging from <1% to >70%, and the majority falling in the 30–60% range, depending on the experimental conditions. Although the trends remained consistent, the solvent and reference compound both had notable impacts on QY. CV revealed some BsubPcs have one reversible reduction and one irreversible or quasi-reversible oxidation, others displayed unique reversibility and/or additional redox processes. The axial groups also influenced the redox potentials, with first oxidation potentials spanning a 194 mV range and first reduction potentials covering a 266 mV range. Electron-withdrawing or electron-donating axial groups impacted the redox behaviour of BsubPcs, suggesting an electronic connection between the axial group and the BsubPc core occurs. This study leads to insights into the axial substituents that should be targeted to be used for other peripherally functionalized BsubPc derivatives for further studies.

Received 19th April 2024,
Accepted 14th May 2024

DOI: 10.1039/d4me00070f

rsc.li/molecular-engineering

Design, System, Application

Boron subphthalocyanines (BsubPcs) are unique organic macrocyclic compounds that are being developed as active materials in organic electronic devices, such as organic photovoltaics (OPVs) and organic light emitting diodes (OLEDs). Organic chemistry enables BsubPc derivatives to be varied through functionalization at the axial and/or peripheral positions. Within the variations of substitutions influences the physical properties of the macrocycle. This study focused on molecular design variations of the axial group. Physical characterization intended to provide insight into relevant properties to take into consideration for further organic electronic applications. A simple, mild, and robust synthetic process was developed to access a structurally diverse array of eighteen axially substituted BsubPcs, starting from Br-BsubPc precursor. This array was then used to systematically study the influence of the axial group on the photophysical and electrochemical properties BsubPcs through UV-vis absorbance and fluorescence spectroscopy also *via* solvent effects, fluorescence quantum yield, cyclic voltammetry, and differential pulse voltammetry to assess their potential for a variety of applications. The results of this study will guide future molecular engineering design of BsubPcs, providing valuable insight into which axial group to target for other peripherally functionalized BsubPcs, as well as the synthetic conditions required to access these derivatives.

[a] *Department of Chemical Engineering and Applied Chemistry, University of Toronto, 200 College Street, Toronto, Ontario, M5S 3E5, Canada. E-mail: tim.bender@utoronto.ca*
[b] *Department of Chemistry, University of Toronto, 80 St. George Street, Toronto, Ontario, M5S 3H6, Canada*
[c] *Department of Materials Science and Engineering, University of Toronto, 184 College Street, Toronto, Ontario, M5S 3E4, Canada*
[d] *Department of Mechanical & Industrial Engineering, University of Toronto, 5 King's College Road, Toronto, Ontario, M5S 3G8, Canada*

† Electronic supplementary information (ESI) available: Full synthetic procedures; structures of the full array of axially substituted BsubPcs; ^{1}H NMR, ^{11}B NMR, mass spectrometry, and HPLC of all investigated BsubPcs; additional normalized absorbance and emission spectra; individual CV and DPV traces of BsubPcs; sublimation temperature profiles for relevant BsubPcs; hot plate temperature calibration curve. See DOI: https://doi.org/10.1039/d4me00070f

Introduction

Organic electronics have garnered considerable attention in recent years due to their potential as low-cost, lightweight, flexible, environmentally benign, and highly customizable alternatives to their silicon-based counterparts.[1–4] Technological advancements in organic electronics are mainly achieved through optimization of device architectures and/or the development of the primary active materials in devices.[5,6] Boron subphthalocyanines (BsubPcs) are a group of macrocyclic dyes being investigated as functional materials in organic electronic devices.[3,5]

BsubPcs are non-planar aromatic organic semiconductors with C_{3v} symmetry and a unique bowl-shaped structure.[3,5,7–14] They are a lower homologue of the phthalocyanine (Pc) family, which are planar molecules consisting of four repeating isoindole units linked by bridging sp^2 nitrogen atoms (Fig. 1a). Pcs can be templated around most metals and metalloids, with boron being one of the exceptions.[5,15] Pcs are commonly used in the dyes and pigments space, but have also found use as organic semiconductors.[3,5] BsubPcs are comprised of a central boron atom surrounded by three repeating isoindole units linked by sp^2 bridging nitrogen atoms (Fig. 1b).[15–17] An additional substituent bonded to the boron atom protrudes from the convex side of the bowl and is known as the axial group/substituent (Fig. 1c).[1,5] The atomic radius of boron is slightly larger than the cavity it occupies, resulting in the characteristic non-planar conformation of the BsubPc macrocycle.[5] Boron is the only element known to template the formation of BsubPcs.[5,16,17]

The unique structure, symmetry, and aromaticity of BsubPcs give rise to rare electronic and photophysical properties that make them attractive for use as active materials in organic electronic devices, such as organic photovoltaics (OPVs) and organic light emitting diodes (OLEDs).[3,5] These properties include absorbance and fluorescence in the visible spectrum; narrow emission profiles; high molar extinction coefficients, redox stability, photostability, and thermal stability; the ability to form thin films; and a low tendency to aggregate due to the bowl-shaped structure and the axial substituent.[1,3,5,9,18–23] BsubPcs tend to have higher solubility compared to planar Pcs and can therefore be incorporated into devices through both solution processing and/or vacuum deposition.[1,22] Furthermore, the ability to tune the properties of BsubPcs through derivatization at the axial and peripheral positions broadens their potential for a variety of applications.[3,5,8,10,17,24–26]

BsubPcs are typically formed through the cyclotrimerization reaction of phthalonitrile in the presence of a trivalent Lewis acidic boron source (Scheme 1).[16,17] Since the first discovery of BsubPcs in 1972, boron trichloride (BCl_3) has been the most commonly used boron source in the synthesis of BsubPcs, resulting in the formation of the prototypical chloro-boron subphthalocyanine (Cl-BsubPc).[16,17,24,27] Cl-BsubPc is useful as both an active material in organic electronics[2,3,5,7,11] and as an intermediate for further axial modification upon reaction.[17,27,28] Boron tribromide (BBr_3) has been used as well, and forms bromo-boron subphthalocyanine (Br-BsubPc), which is most commonly used as an intermediate for other axially substituted BsubPcs due to the thermodynamic nature of the boron–bromine bond.[17,29,30]

As previously mentioned, there are two primary methods of altering the properties of BsubPcs: derivatization at the axial position and derivatization at the peripheral positions. Substitution around the periphery of the BsubPc macrocycle is typically accomplished by functionalization of the phthalonitrile precursor prior to the formation of the macrocycle, while axial derivatization is accomplished through substitution of the axial halide after the macrocycle has been formed (Scheme 1).[17,22,31] The synthetic possibilities for axial modification far exceed that of peripheral functionalization, and for that reason, the axial group was targeted in this study.

When designing functional materials for an organic electronic application, it is important to identify the properties of interest for specific applications. Fluorescence quantum yield (Φ_f or QY) is one such example. QY is a measure of the fluorescence efficiency of a compound, defined as the ratio of the number of photons emitted (N_{em}) by a chromophore to the number of photons absorbed (N_{abs}) (eqn (1)).[32,33]

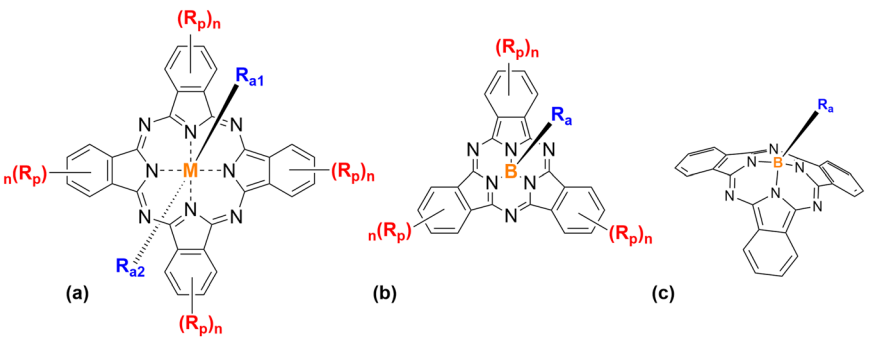

Fig. 1 a) General molecular structure of phthalocyanine (Pc) where R_{a1} and R_{a2} denote the axial positions and R_p denotes the peripheral positions, b) general 2D molecular structure of boron subphthalocyanine (BsubPc) where R_a denotes the axial position and R_p denotes the peripheral positions, and c) general 3D structure of BsubPc showing the bowl-shaped structure with R_a representing the axial position.

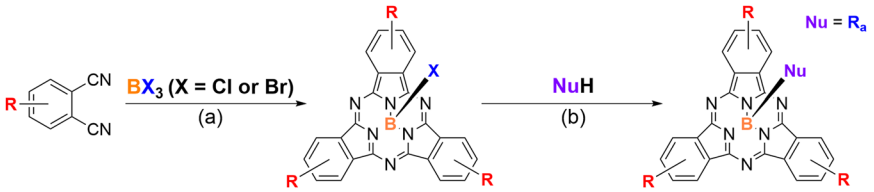

Scheme 1 General synthesis of boron subphthalocyanine and axial exchange reaction with a general nucleophile. [a]Conditions for R = H; 2.4 equivalents of BCl_3 (1.0 M in heptane) in 1,2-dichlorobenzene at reflux for 1.5 hours for X = Cl, or 0.33 equivalents of BBr_3 in bromobenzene/toluene at room temperature overnight for X = Br. [b]General literature conditions, 5–10 equivalents of the nucleophile (NuH) in refluxing toluene, chlorobenzene, or dichlorobenzene. Conditions vary based on desired axial group and original axial halide.

$$\Phi_f = \frac{N_{em}}{N_{abs}} \quad (1)$$

Molecules with a high quantum yield are those that relax and light emit primarily through radiative mechanisms, resulting in the emission of light. For emissive devices like OLEDs, the efficiency with which their active material(s) radiatively relax from an excited state is incredibly important to the performance of the device.[32,33] Relative QY is the more established and widely used method in the field, using common absorbance and fluorescence spectrometers.[33,34] The limitations with the relative QY method are primarily related to the availability of a reference compound that has a reliable, well-characterized quantum yield value, and has absorption and emission spectra that are similar to the compound of interest.[33,34]

Electrochemical characterization is another useful tool for evaluating BsubPcs for organic electronic applications. The alignment of the frontier molecular orbitals of the electron donor and acceptor materials in OPVs is a crucial factor for optimal device application.[25,26] Cyclic voltammetry can be used to estimate the highest occupied molecular orbital (HOMO) and lowest unoccupied molecular orbital (LUMO) energy levels, with oxidation and reduction events being related to the HOMO and LUMO, respectively.[5,35] Furthermore, the reversibility and potential(s) of the oxidation and reduction potentials indicate whether a material is more suitable as an electron donor or electron acceptor. BsubPcs were originally studied as electron donors within OPVs, but alternatives has enabled the HOMO and LUMO levels to be shifted such that BsubPcs could be used as non-fullerene electron acceptors as well.[3] From a sustainability standpoint, fullerene-free devices are desirable due to the lower embodied energy of BsubPcs compared to fullerene.[36,37]

The results of electrochemical characterization are highly sensitive to the experimental conditions under which they are measured.[35] Therefore, compounds can only be compared if they have been characterized under matching conditions. Similarly, in the BsubPc space, many different solvents, reference compounds, and excitation wavelengths have been reported for quantum yield.[22] Therefore, there has yet to be a study exploring the influence of different experimental parameters on the quantum yield of BsubPcs.

A comprehensive investigation comparing the photophysical and electrochemical properties of BsubPcs with a wide range of axial groups under identical experimental conditions has yet to be studied. Therefore, within this study, the influence of the axial group on the photophysical and electrochemical properties of BsubPcs was investigated, while the periphery was left unsubstituted (*i.e.* only hydrogen atoms). The axial position has mostly been used as a synthetic handle to influence properties such as solubility,[26,38,39] crystal structure,[26,40–42] sublimation temperature,[43] and stability.[5,23] The axial position has not generally been considered to have as significant an impact on the optical and electronic properties of BsubPcs as peripheral substitution due to the axial ligand being separated from the conjugated system that is largely responsible for these properties.[5,13,16] However, past studies have largely focused on comparing the photophysical and/or electronic properties of a small subset of structurally similar axial group substituents, such as halides,[22,29,44] phenoxy derivatives,[22,25–27,38] or phenyl derivatives;[22,45] or have been limited to the synthesis of particular BsubPc derivatives using novel synthetic methods.[21,46,47] Moreover, certain axial groups have resulted in unique electrochemical behaviour,[26,28] and even within the halides there is a significant effect on quantum yield (QY).[29] Therefore, our desire was to study further the influence of the BsubPc axial group to understand the full scope of its impact on these critical physical properties.

This study marks the first example of a systematic comparison of the photophysical and electrochemical properties of a structurally diverse array of axially substituted BsubPcs under identical experimental conditions.[25] An array of eighteen axially substituted BsubPcs consisting of halide (**1a**,**b**), alkoxy (**2a–f**), phenoxy (**3a**,**b**), carboxylate (**4a**,**b**), hydroxy (**5**), siloxy (**6**), phenyl (**7**), thiophenoxy (**8a**,**b**), and amino (**9**) derivatives (Fig. 2) were synthesized, purified, and characterized by solution-state UV-vis absorbance and fluorescence, relative fluorescence quantum yield (QY), cyclic voltammetry (CV), and differential pulse voltammetry (DPV). Photophysical characterization was conducted in toluene and α,α,α-trifluorotoluene (also called trifluorotoluene or F_3-toluene), and relative QY values were referenced to previously well-characterized reference standards of F_5-BsubPc[10] and PhO-F_{12}BsubPc.[8] The results of this investigation will provide

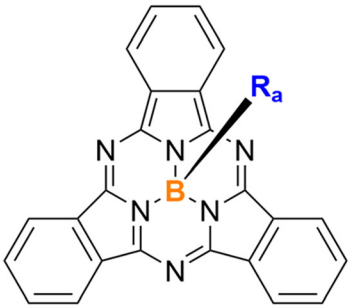

#	R_a Name	R_a Structure	#	R_a Name	R_a Structure
1a	Chloro (Cl)		3b	β-Naphthoxy (naphthoxy)	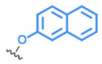
1b	Fluoro (F)		4a	Acetate	
2a	Methoxy (MeO)	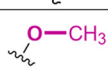	4b	Benzoate	
2b	Ethoxy (EtO)	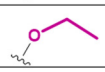	5	Hydroxy (HO)	
2c	Trifluoroethoxy (F_3EtO)		6	Trimethylsiloxy (TMSO)	
2d	Butoxy (ButO)		7	Phenyl (Ph)	
2e	Tertbutoxy (tButO)		8a	Pentafluorothiophenoxy (F_5PhS)	
2f	Octoxy (OctO)		8b	4-methylthiophenoxy (MePhS)	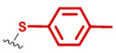
3a	Phenoxy (PhO)	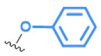	9	*N*-phenyl-*N*-methyl-amino (PhMeN)	

Fig. 2 Structures of the BsubPc axial substituents investigated in this study, with R_a representing the axial group.

valuable insight into which axial groups to target when designing other peripherally functionalized BsubPcs for specific applications in upcoming studies.

Experimental

Materials

Toluene, methanol, hexanes, pentane, acetone, chloroform, ethyl acetate, dimethyl sulfoxide, acetonitrile (HPLC-grade), *N*,*N*-dimethylformamide (distilled in glass), phenol, pentafluorophenol, acetic acid (glacial), and standard basic alumina were purchased from Caledon Laboratories (Caledon, Ontario, Canada) and used as received. Bromobenzene, chlorobenzene (anhydrous), tetrahydrofuran (anhydrous), absolute ethanol, 2,2,2-triflouroethanol, 1-butanol, *tert*-butanol, 1-octanol, 1,2-dichlorobenzene, α,α,α-trifluorotoluene, 1,2-dichloroethane, hexamethylphosphoramide, boron tribromide, boron trichloride (1.0 M in heptane), phenylmagnesium bromide (1.0 M in THF), benzoic acid, trimethylsilanol, *N*-methylaniline, 2-naphthol, tetrabutylammonium perchlorate, and ferrocene (98%) were purchased from Sigma-Aldrich Chemical Company (Mississauga, Ontario, Canada) and used as received. Phthalonitrile, *p*-toluenethiol, and pentafluorothiophenol were purchased from TCI America (Portland, Oregon) and used as received. Chloroform-d_1 was purchased from Cambridge Isotopes Laboratories, Inc. (Massachusetts, USA). Aluminum plates coated with aluminum oxide were purchased from Chromatographic Specialties Inc. (Brockville, Ontario, Canada).

Instrumentation and methods

High-performance liquid chromatography (HPLC). HPLC analysis was conducted using a Waters 2695 separation module with a Waters 2998 photodiode array and a SunFire™ C18 3.5 μm 3.0 × 150 mm column. HPLC-grade acetonitrile (ACN) and distilled in glass *N*,*N*-dimethylformamide (DMF) were used as the mobile phase eluted at 0.6 mL min^{-1} at a composition of 80 : 20 (v : v). A mobile phase composition of 95 : 5 (v : v) ACN/DMF was used in some cases during reaction monitoring to increase the separation between compounds with similar retention times, as outlined in the ESI.†

UV-vis spectroscopy. Solution-state ultraviolet-visible (UV-vis) spectroscopy was conducted at room temperature in toluene and α,α,α-trifluorotoluene with a PerkinElmer LAMBDA 1050 spectrophotometer using a PerkinElmer quartz cuvette with a 10 mm path length. A scan range of 850 to 200 nm was used with a data interval of 0.5 nm. UV-vis absorption measurements were taken in triplicate for each compound in each solvent, and the maximum absorption wavelength (λ_{max}^{abs}) determined by averaging the three scans.

Fluorescence spectroscopy. Photoluminescence (PL) spectra were measured in toluene and α,α,α-trifluorotoluene at room temperature using a PerkinElmer LS-55 fluorescence spectrometer and a PerkinElmer quartz cuvette with a 10 mm path length, a scan range of 200 to 850 nm, an excitation slit width of 10 nm, an emission slit width of 10 nm, and a scan speed of 250 nm min^{-1}. The reported fluorescence spectra and maximum emission wavelengths (λ_{max}^{em}) were acquired for each compound in each solvent using an excitation wavelength (λ_{ex}) equal to the maximum absorption wavelength of the compound in toluene ($\lambda_{max,tol}^{abs}$) minus 45 (eqn (2)).

$$\lambda_{ex} = \lambda_{max,tol}^{abs} - 45 \quad (2)$$

Fluorescence quantum yield. Relative fluorescence quantum yield (Φ_f or QY) was calculated using eqn (3).[33]

$$\Phi_f = \Phi_R\left(\frac{I}{I_R}\right)\left(\frac{OD_R}{OD}\right)\left(\frac{n^2}{{n_R}^2}\right) \quad (3)$$

where Φ_f is the unknown fluorescence quantum yield of the compound of interest, Φ_R is the known fluorescence quantum yield of the reference compound, I is the integrated fluorescence intensity (*i.e.* the area under the emission curve), OD is the optical density (*i.e.* the absorbance at the excitation wavelength), and n is the refractive index of the solvent(s). The subscript R refers to the reference compound.[33] Fluorescence quantum yields were measured at room temperature in toluene and α,α,α-trifluorotoluene. pentafluorophenoxy-boron subphthalocyanine (F_5-BsubPc), with a previously well-characterized quantum yield of 0.42 (ref. 10) in toluene at room temperature, and phenoxy-dodecafluoroboron subphthalocyanine (PhO-F_{12}BsubPc), with a previously well-characterized quantum yield of 0.40 (ref. 8 and 10) in toluene at room temperature, were used as reference compounds. Dilute solutions of each compound in both solvents were prepared and their absorption spectra recorded. Solutions were prepared with maximum absorbance between 0.04 and 0.05 AU.[33] UV-vis measurements taken in triplicate and averaged were used in the calculation of quantum yield. Fluorescence data was acquired with excitation wavelengths equal to the maximum absorption wavelength of each compound in toluene ($\lambda^{abs}_{max,tol}$) minus 45 (eqn (2)). QY measurements in toluene were run twice for each axially substituted BsubPc and the two reference compounds. QY was calculated for both runs of each BsubPc with respect to both runs of each reference compound. This resulted in four QY values being calculated for each BsubPc with respect to each reference compound in toluene. The reported QY values in toluene with respect to each reference compound are the average of the four values. QY measurements were run once in α,α,α-trifluorotoluene and calculated with respect to both runs of each reference compound in toluene, resulting in two QY values being calculated for each BsubPc in α,α,α-trifluorotoluene with respect to each reference compound. The reported QY values in α,α,α-trifluorotoluene are the average of the two values. The error in the QY values is reported as the standard error (SE) (eqn (4)).

$$SE = \frac{\sigma}{\sqrt{n}} \quad (4)$$

where σ is the standard deviation and n is the number of samples (n = 4 for toluene, n = 2 for α,α,α-trifluorotoluene).

Electrochemistry. Cyclic voltammetry (CV) and differential pulse voltammetry (DPV) were conducted using a Basi EC-Epsilon potentiostat/galvanostat with the C3 cell stand. All samples were run at room temperature in nitrogen-degassed dichloromethane (DCM) solutions of 0.1 M tetrabutylammonium perchlorate (TBAP) as the supporting electrolyte. A 20-minute nitrogen purge was applied prior to experimentation. Ferrocene was used as the internal reference. A conventional three-electrode system was used with a 1 mm platinum disk as the working electrode, a platinum wire as the counter electrode, and Ag/AgCl in 3 M sodium chloride salt solution as the reference electrode. For CV, samples were analyzed over a range of +1.6 to −1.6 V at a scan rate of 100 mV s^{-1} for three full cycles. CV potentials were corrected to the half-wave oxidation potential of ferrocene (FC/FC^+) ($E_{1/2,ox}$ = 0.547 V *vs.* Ag/AgCl).[35,48] For DPV, scan windows of +0.10 to +1.6 V and +0.80 to −1.6 V were used with a pulse amplitude of 0.05 V. All DPV potentials were corrected to the maximum potential of ferrocene, which was calculated to be 0.522 V *vs.* Ag/AgCl using the following equation: $E_{max} = E_{1/2} - \frac{\Delta E}{2}$, where E_{max} is the maximum potential, $E_{1/2}$ is the known half-wave potential, and ΔE is the pulse amplitude.[49]

Nuclear magnetic resonance spectroscopy. 1D proton (^{1}H) and boron (^{11}B) nuclear magnetic resonance (NMR) spectra were obtained from a 400 MHz Bruker Avance III NMR spectrometer. ^{1}H spectra are referenced to the deuterated solvent peak ($CDCl_3$, δ_H = 7.26 ppm).

Mass spectrometry. Direct analysis in real time high-resolution mass spectrometry (DART-HRMS) was conducted using a JEOL AccuTOF-DART in positive ion mode.

Synthesis of boron subphthalocyanines. Detailed synthetic procedures for Br-BsubPc, Cl-BsubPc, and all axially substituted BsubPcs are provided in the ESI.†

Results and discussion

The goal of this study was to systematically investigate the influence of a diverse array of axial substituents on the photophysical and electrochemical properties of boron subphthalocyanines (BsubPcs). Each compound was synthesized and purified to a yield and purity that was appropriate for physical characterization.

Synthesis of axially substituted BsubPcs

Eighteen axially substituted BsubPcs were synthesized in this study. With the exception of chloro-boron subphthalocyanine (Cl-BsubPc), all compounds were synthesized through an axial exchange reaction between bromo-boron subphthalocyanine (Br-BsubPc) and the appropriate nucleophile for the desired axial substituent. Cl-BsubPc and Br-BsubPc have both been previously used as an intermediate for axial exchange reactions. The axial boron–chlorine bond is more stable than the boron–bromine bond, and it is less susceptible to hydrolysis to form hydroxy-boron subphthalocyanine (HO-BsubPc) during work-up, purification, and/or storage.[17,30] However, the higher stability also means that axial exchange reactions with Cl-BsubPc are slower kinetics wise than with Br-BsubPc due to the higher activation energy of the reaction,[29,50] and Cl-BsubPc needs higher activational energy or no reaction occurs with certain

nucleophiles without the use of supplementary reagents/catalysis to generate activated BsubPc intermediates.[16,17,21,46] The lower reactivity of the B–Cl bond also tends to lead to long reaction times at very high temperatures, which could also result in degradation of the macrocycle.[16,22,25,46] Based on the higher reactivity of Br-BsubPc, as well as the recent report from our group that Br-BsubPc has a higher potential for scale-up than Cl-BsubPc,[51] Br-BsubPc was chosen as the template for all axial exchange reactions in this study.

Screening reactions. There are several methods in the literature for axial exchange reactions, with specific reaction conditions varying based on the axial group being targeted to exchange with the starting axial halide.[2,5,8,10,21,25,26,28,38,45,46,52,53] Guided by these previously reported methods, a Heidolph Carousel 6 Plus™ Reaction Station was used for our study to quickly screen various solvents, molar ratios, and temperatures in small-scale reactions to develop a general set of axial exchange reaction conditions. From an engineering perspective, the goal was to establish a robust procedure with mild reaction conditions that could be applied to as many nucleophiles as possible. Reaction progress was monitored by HPLC.

All screening reactions were run with 115 mg of Br-BsubPc and 2.5 mL of solvent. A temperature calibration of the reaction station was conducted to correlate the external temperature to the internal reaction temperature. The first optimization step was to study twelve solvents for phenoxylation reactions, whereby Br-BsubPc was reacted with 5 equivalents of phenol at 35 °C (internal). Complete conversion of Br-BsubPc occurred the fastest when chlorinated solvents (chlorobenzene, dichloromethane, chloroform, and dichloroethane) were used (Table 1). Therefore, chlorobenzene was chosen to use as the axial exchange reaction solvent due to its high boiling point compared to the other investigated chlorinated solvents (Table 1), allowing for higher reaction temperatures if needed for less reactive nucleophiles moving forward.

The molar equivalency of the nucleophile was tested next. Three nucleophiles (phenol, pentafluorophenol, and *p*-toluenethiol) were tested at 2 and 5 equivalents in axial exchange reactions in chlorobenzene at 35 °C (internal) to form PhO-BsubPc, F_5-BsubPc, and MePhS-BsubPc, respectively (Fig. S1†). Phenol reacted quickly with both 2 and 5 equivalents, reaching full conversion of Br-BsubPc in 2 hours and 1 hour, respectively. The reaction with 5 equivalents of pentafluorophenol reached full conversion of Br-BsubPc in 29 hours, but 2 equivalents only reached ~98% conversion after 69 hours. No reaction was observed with *p*-toluenethiol with either molar equivalency, demonstrating the lower reactivity of sulfur-based nucleophiles compared to oxygen-based nucleophiles. The molar equivalency experiments were repeated at 75 °C (internal). The reactions with 2 equivalents of phenol and 5 equivalents of phenol and pentafluorophenol went to completion by the time the reaction temperature was reached. With 2 equivalents of pentafluorophenol, full conversion of Br-BsubPc was seen in 1 hour. Reactions with both 2 and 5 equivalents of *p*-toluenethiol reached ~90% conversion of Br-BsubPc after 50 hours. To our knowledge, this is the first observation of a successful axial exchange reaction with a sulfur-based nucleophile without first activating the axial halide bond with an auxiliary reagent such as aluminum chloride ($AlCl_3$)[21] or silver triflate (AgOTf).[46] Furthermore, the reaction occurred under relatively mild conditions, with a moderate temperature of 75 °C (internal) and an equal molar equivalence of the nucleophile as what is commonly seen in the literature for oxygen-based nucleophiles.[10,26,27,38] This demonstrates that extreme reaction conditions may not be required for sulfur-based nucleophiles to react. This result further justifies the use of Br-BsubPc as the template for axial exchange reactions in this study. The results of the molar equivalency tests at both temperatures are summarized in Table 2.

Based on the combinatorial screening results, the general axial exchange reactions conditions include 5 equivalents of the nucleophile, chlorobenzene as the reaction solvent, and a reaction temperature of 75 °C (internal). These conditions are milder than many of the previously reported methods,

Table 1 Summary of the solvent screening kinetic results

Solvent	Reaction time[a] (h)	Boiling point (°C)
Chlorobenzene	1.5	132
Dichloromethane	1.5	40
Chloroform	1.5	61
Dichloroethane	1.5	83
Toluene	3	110
Acetone	53	56
Acetonitrile	>69	82
Tetrahydrofuran	70	66
DMSO	>73	189
DMF	>73	153
Ethyl acetate	>73	77
HMPA	>73	233

[a] Reaction time indicates time to full conversion of Br-BsubPc as monitored by HPLC.

Table 2 Summary of the molar equivalence and temperature screening kinetic results

Nucleophile	Molar equivalence	Reaction time[a] (h)
Reaction temperature: 35 °C		
Phenol	2	2
	5	1
pentafluorophenol	2	>69
	5	29
p-Toluenethiol	2	No reaction
	5	No reaction
Reaction temperature: 75 °C		
Phenol	2	<0.5 h
	5	<0.5 h
pentafluorophenol	2	2
	5	<0.5 h
p-Toluenethiol	2	>50 h
	5	>50 h

[a] Reaction time indicates time to full conversion of Br-BsubPc as monitored by HPLC.

most of which are run at reflux in toluene (110 °C), chlorobenzene (132 °C), or 1,2-dichlorobenzene (180 °C).[17]

Scale-up and purification. The reaction conditions established above were applied on the 0.5 g or 1.0 g scale to synthesize the axially substituted BsubPcs (Fig. S1†) that were purified and characterized for the study of physical properties. Minor adjustments were made to the reaction conditions based on the reactivity of the various nucleophiles. Molar equivalence of the nucleophile was the primary variable that was changed, as the axial exchange reaction was previously reported by Guilleme *et al.* to be bimolecular in nature.[54] Once synthesized, the axially substituted BsubPcs were purified by train sublimation or column chromatography on standard basic alumina. Train sublimation is the preferred method of purification because solvent-free purification methods are more sustainable and environmentally friendly than chromatographic purification methods, which tend to require large volumes of solvent. Furthermore, purification by train sublimation generally resulted in higher product recoveries than chromatography methods (Table 3). The purity and structures of the axially substituted BsubPcs were confirmed by HPLC, NMR, and mass spectrometry (Fig. S2–S93).†

The oxygen-based nucleophiles tended to react the quickest, with reactions generally going to completion between 1 hour and overnight with 5–10 equivalents of the nucleophile (Scheme 2). In some cases, the reactions stalled overnight, so an additional dosing of the nucleophile was added. PhO- (**3a**), naphthoxy- (**3b**), acetate- (**4a**), benzoate (**4b**), EtO- (**2b**), F_3EtO- (**2c**), ButO- (**2d**), and OctO-BsubPc (**2f**),

Table 3 Summary of the axial exchange reaction results

Axial group	Crude yield[a]	Crude purity[b]	Purification method	Purification recovery[a]	Final purity[b]
Cl (**1a**)	33%	>99%	Sublimation (405 °C)	63%	99.4%
F (**1b**)	118%	97.7%	2× sublimation (420 °C)	25%, 94%	99.6%
MeO (**2a**)	73%	95.5%	Sublimation (300 °C)	46%	>99.9%
EtO (**2b**)	72%	98.4%	Sublimation (295 °C)	33%	99.4%
F_3EtO (**2c**)	63%	94.4%	Sublimation (305 °C)	58%	99.9%
ButO (**2d**)	109%	96.7%	Sublimation (265 °C)	31%	99.7%
*t*ButO (**2e**)	100%	63.0%	Chromatography[e]	30%[d]	99.2%[c]
OctO (**2f**)	45%	97.9%	Sublimation (275 °C)	20%	98.6%
PhO (**3a**)	53%	97.5%	Sublimation (330 °C)	67%	99.7%
Napthoxy (**3b**)	66%	98.2%	Sublimation (315 °C)	40%	>99.9%
Acetate (**4a**)	90%	97.7%	Sublimation (290 °C)	58%	99.3%
Benzoate (**4b**)	112%	93.9%	Sublimation (355 °C)	45%	99.1%
HO (**5**)	104%	95.7%	Sublimation (420 °C)	4%	99.9%
TMSO (**6**)	90%	65.8%	Chromatography[f]	7%	>99.9%
Ph (**7**)	111%	16.3%	Chromatography[g]	6%	89.0%
F_5PhS (**8a**)	69%	45.6%	Chromatography[f]	4%	98.1%
MePhS (**8b**)	83%	71.9%	Chromatography[h]	2%	98.5%
PhMeN (**9**)	58%	49.0%	Chromatography[e]	13%[d]	99.6%[c]

[a] Yield and recovery calculated based on mass collected. [b] Purity based on HPLC analysis with a mobile phase of 80 : 20 ACN/DMF. [c] Average purity of 2 "crops" of product. [d] Combined recovery of 2 "crops" of product. [e] 5 : 1 DCM/hexanes, standard basic alumina. [f] 1 : 1 DCM/hexanes, standard basic alumina. [g] 2 : 1 DCM/hexanes, standard basic alumina. [h] 100% DCM, standard basic alumina.

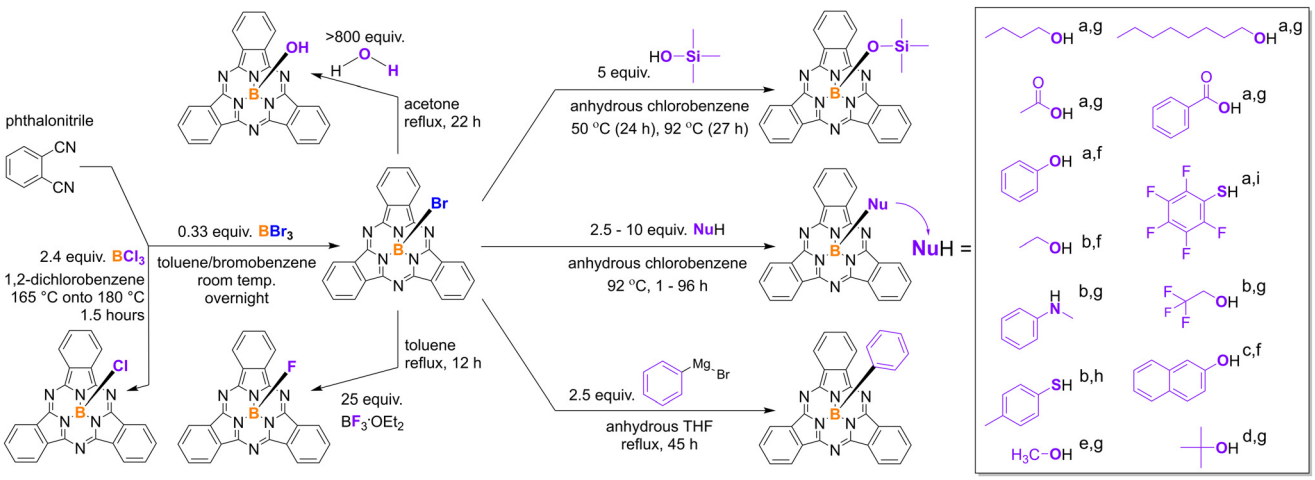

Scheme 2 Synthetic pathways for Br-BsubPc and axial exchange reactions. [a]5 equivalents. [b]10 equivalents. [c]2.5 equivalents. [d]2 × 10 equivalents. [e]1 × 10 equivalents, 1 × 5 equivalents, 1 × 23.5 equivalents. [f]1–4.5 h. [g]22–28 h. [h]44 h. [i]96 h.

outlined in Fig. 1, all formed quickly with relatively high crude yields and purities, and were purified by train sublimation at much lower temperatures (265–355 °C) than are typically required for axially and/or peripherally halogenated BsubPcs (>400 °C) (Table 3).

The reactions to form MeO-BsubPc (**2a**) and *t*ButO-BsubPc (**2e**) both stalled at 95–98% conversion of Br-BsubPc after initially reacting quickly. However, it was found that the first attempt to purify MeO-BsubPc by train sublimation (330 °C) was unsuccessful, resulting in co-deposition of MeO-BsubPc with HO-BsubPc, μ-oxo-BsubPc, and a small amount of unreacted Br-BsubPc. This result motivated the further optimization of the process to use a large excess of methanol in subsequent experiments to push the reaction to full conversion (Scheme 2). MeO-BsubPc was then successfully purified by train sublimation at 300 °C, with HO-BsubPc and μ-oxo-BsubPc remaining in the metal boat rather than co-depositing with MeO-BsubPc. Purification of *t*ButO-BsubPc by train sublimation was unsuccessful due to the relatively low purity of the crude material, resulting in co-deposition with undesired BsubPcs. Successful purification of *t*ButO-BsubPc was accomplished by column chromatography.

HO-BsubPc (**5**) was synthesized following a procedure adapted from Paton and Bender (Scheme 2).[53] This reaction was run at reflux in acetone (56 °C) overnight to reach full conversion of Br-BsubPc, resulting in a crude product with high yield and purity. During train sublimation, most of the HO-BsubPc formed μ-oxo-BsubPc (an oxygen-bridged BsubPc dimer), resulting in a low sublimation yield. Still, a sufficient amount of high-purity sublimed HO-BsubPc was recovered for characterization.

Next, the reaction of Br-BsubPc with trimethylsilanol to form TMSO-BsubPc (**6**) resulted in the lowest conversion of Br-BsubPc observed in this study. Under a variety of reaction conditions, Br-BsubPc conversion stalled at ~50–70%. At 92 °C (external), Br-BsubPc conversion stalled at ~60%. When the reaction was run for longer than 50 hours, the product started to degrade through hydrolysis to HO-BsubPc or through the formation of μ-oxo-BsubPc. At both room temperature and 50 °C, Br-BsubPc conversion stalled at ~50%, even with an additional dosing of the nucleophile. To try to maximize conversion without the product degrading, the reaction was run at 50 °C (external) overnight (~24 h), and then the temperature was increased to 92 °C (external) overnight (~27 h), for a total reaction time of 51 hours (Scheme 2). Approximately 70% conversion of Br-BsubPc was achieved under these conditions, with HO-BsubPc and μ-oxo-BsubPc just starting to form ~50 hours into the reaction. Purification by train sublimation largely resulted in co-deposition of TMSO-BsubPc with Br-BsubPc, HO-BsubPc, and μ-oxo-BsubPc. Therefore, for purification of TMSO-BsubPc, column chromatography was used and was more successful in this case to justify taking the material forward for the physical property characterization.

Next, a different set of reaction conditions were used to synthesize Ph-BsubPc (**7**) due to the use of a Grignard reagent as the nucleophile (Scheme 2). The procedure reported by Bonnier *et al.*[45] uses 2 equivalents of phenylmagnesium bromide and the reaction is stirred at reflux for 16 hours. This method resulted in only ~50% conversion of Br-BsubPc to Ph-BsubPc. As previously observed, 4-bromobutoxy-BsubPc formed as a by-product due to the ring-opening and subsequent reaction of the THF reaction solvent with Br-BsubPc.[45,55] In our case, this undesired by-product formed as the major product, with minimal Ph-BsubPc forming. Increasing the equivalence of phenylmagnesium bromide to 2.5 was the next step, and resulted in full conversion of Br-BsubPc, but 4-bromobutoxy-BsubPc was still the major product. Additionally, the ratio of 4-bromobutoxy-BsubPc to Ph-BsubPc seemed to increase over time as the reaction ran. This may occur due to the higher thermodynamic stability of the boron–oxygen axial bond compared to the boron–carbon axial bond. It is unclear why 4-bromobutoxy-BsubPc was consistently formed preferentially over the desired Ph-BsubPc product in our case, but not in previous reports. Separation and purification were successfully achieved by column chromatography on standard basic alumina. The final purity of Ph-BsubPc was lower than the other axially substituted BsubPcs at 89.0%. None of the impurities present in the sample were BsubPcs, nor were they UV active (Fig. S74†). Therefore, the impurities did not interfere with the photophysical characterization. Moreover, the purity of Ph-BsubPc was sufficient enough for electrochemical characterization, as none of the impurities were present in a large enough quantity to interfere with the measurements.

The two thiophenoxy derivatives, F_5PhS-BsubPc (**8a**) and MePhS-BsubPc (**8b**), both formed successfully, marking the first reports of direct axial substitution with sulfur-based nucleophiles without the use of auxiliary reagents to activate the boron–halide bond.[21,46] These reactions were slow compared to the others in this study, particularly with pentafluorothiophenol, and the yield of the final products after purification was very low (Table 3). Still, both products were successfully purified by chromatography on standard basic alumina, and a sufficient amount of pure material was collected for justification of the physical characterization.

PhMeN-BsubPc (**9**) formed with relative ease, despite past reports stating no reaction occurs with *N*-methylaniline.[17,21] Past unsuccessful attempts used Cl-BsubPc as the template for the axial exchange reaction,[21] further demonstrating the utility of Br-BsubPc as an intermediate for axial functionalization with a wider range of nucleophiles. In our hands, the reaction went to completion overnight using 10 equivalents of *N*-methylaniline (Scheme 2). The crude purity was quite low compared to the B–O bonded BsubPcs (Table 3), but the product was successfully purified by column chromatography on standard basic alumina. This is the first report of a direct axial substitution using a non-phthalimide nitrogen-based nucleophile.

Photophysical characterization

UV-vis absorption and emission. UV-vis absorption and emission measurements for each compound were taken at

room temperature in toluene and α,α,α-trifluorotoluene to study the solvent effects in addition to the influence of the axial group. The characteristic absorption spectrum of BsubPcs has consistent of a maximum absorbance band in the visible region, called the Q-band, and a broad peak in the UV region, named as the Soret band. The Q-band is attributed to a $S_0 \rightarrow S_1$ transition, the Soret band arises from a $S_0 \rightarrow S_2$ transition,[16,17] and the shoulder peaks of the Q-band are attributed to vibrational transitions.[17]

Consistent with previous reports, the axial group has a minimal impact on the absorption and emission peaks of BsubPcs (Fig. 3).[26,29] This is because the axial group is separated from the conjugated macrocyclic core that is largely responsible for these phenomena in BsubPcs (Fig. 2).

When measured in toluene, the maximum absorption wavelengths ($\lambda^{abs}_{max,tol}$) of the eighteen axially substituted BsubPcs all fell within 9 nm of each other, ranging from 560–569 nm (Table 4). The heteroatom bonded to boron and electron-donating *vs.* electron-withdrawing effects within the axial functional groups were the main factors causing the slight shifts in the BsubPc absorbance spectra. F-BsubPc (**1b**) and ten of the twelve compounds with boron–oxygen bonds, including the six alkoxy-BsubPcs (**2a–f**), two phenoxy-BsubPcs (**3a,b**), HO-BsubPc (**5**), and TMSO-BsubPc (**6**), were the most blue-shifted of the axially substituted BsubPcs, all having $\lambda^{abs}_{max,tol}$ between 560–562 nm. The two carboxylate derivatives, acetate-BsubPc (**4a**) and benzoate-BsubPc (**4b**), displayed slightly red-shifted absorbance spectra compared to the other axial B–O bonded BsubPcs, with $\lambda^{abs}_{max,tol}$ of 564 nm and 565 nm, respectively. This is likely a result of the electron withdrawing effects of the carbonyl group. A similar result was seen with the 1 nm redshift of F_3EtO-BsubPc (**2c**) compared to EtO-BsubPc (**2b**) due to the three electron-withdrawing fluorines, as well as with the 3 nm redshift of F_5PhS-BsubPc (**8a**) compared to MePhS-BsubPc (**8b**) due to five electron-withdrawing fluorines on **8a** compared to the electron donating methyl group on **8b**. The slight redshift of Cl-BsubPc (**1a**, $\lambda^{abs}_{max,tol}$ = 565 nm) compared to F-BsubPc (**1b**) is consistent with previous observations.[29] PhMeN-BsubPc (**9**), the only investigated compound with an axial boron–nitrogen bond, has a maximum absorbance of 564 nm, similar to the carboxylate derivatives (**4a,b**) and Cl-BsubPc (**1a**). The BsubPcs with axial boron–carbon (**7**) and boron–sulfur (**8a,b**) bonds have the most redshifted absorbance

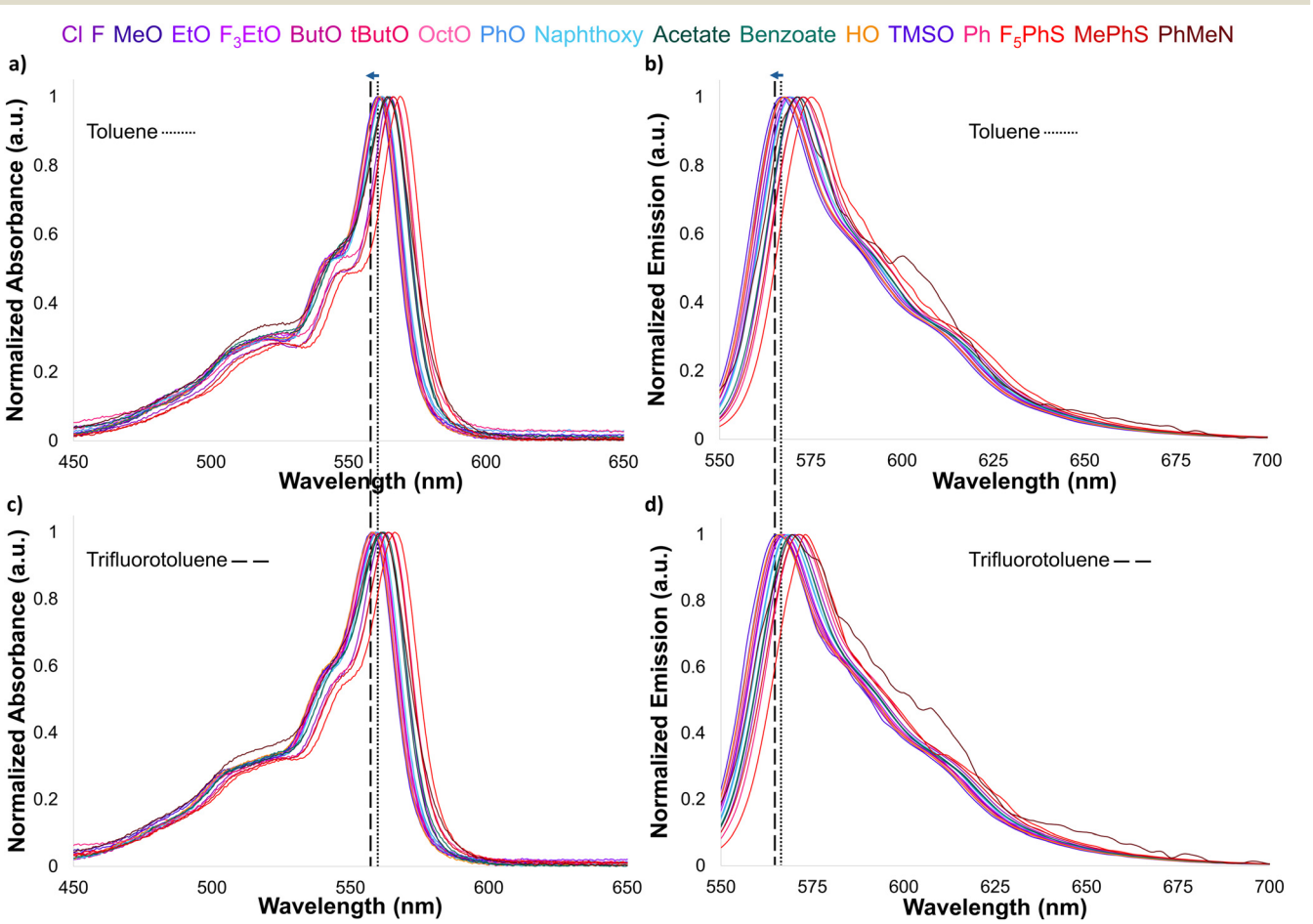

Fig. 3 Normalized a) UV-vis absorbance spectra in toluene, b) emission spectra in toluene, c) UV-vis absorbance spectra in α,α,α-trifluorotoluene, d) emission spectra in α,α,α-trifluorotoluene for all axially substituted BsubPcs. Dotted and dashed lines represent the most blue-shifted absorbance and emission spectra in toluene and α,α,α-trifluorotoluene, respectively.

Table 4 Maximum absorbance and emission wavelengths, quantum yields, and stokes shifts of the array of axially substituted BsubPcs in toluene and α,α,α-trifluorotoluene

		Toluene					α,α,α-Trifluorotoluene				
Axial group	λ_{ex}[a] (nm)	λ_{max}^{abs} (nm)	λ_{max}^{em} (nm)	Stokes shift (nm)	$\Phi_{f,F_5\text{-BsubPc}}$	$\Phi_{f,PhO\text{-}F_{12}BsubPc}$	λ_{max}^{abs} (nm)	λ_{max}^{em} (nm)	Stokes shift (nm)	$\Phi_{f,F_5\text{-BsubPc}}$	$\Phi_{f,PhO\text{-}F_{12}BsubPc}$
Cl (**1a**)	520	565	571.5	6.5	0.68 ± 0.03	0.74 ± 0.02	562	570	8	0.60 ± 0.02	0.66 ± 0.02
F (**1b**)	517	562	569	7	0.50 ± 0.01	0.59 ± 0.01	559	567	8	0.44 ± 0.02	0.49 ± 0.01
MeO (**2a**)	517	562	567.5	5.5	0.47 ± 0.01	0.53 ± 0.01	558	566	8	0.39 ± 0.01	0.44 ± 0.01
EtO (**2b**)	516	561	568	7	0.46 ± 0.01	0.54 ± 0.01	558.5	566	7.5	0.42 ± 0.02	0.48 ± 0.01
F_3EtO (**2c**)	517	562	569.5	7.5	0.44 ± 0.02	0.50 ± 0.01	559.5	567.5	8	0.37 ± 0.01	0.41 ± 0.01
ButO (**2d**)	516	561	568	6.5	0.50 ± 0.02	0.58 ± 0.01	558.5	566	7.5	0.41 ± 0.02	0.48 ± 0.01
*t*ButO (**2e**)	517	562	568	6	0.48 ± 0.01	0.54 ± 0.01	559	566.5	7.5	0.40 ± 0.01	0.45 ± 0.01
OctO (**2f**)	516	561	567.5	6.5	0.49 ± 0.01	0.57 ± 0.01	558.5	566	7.5	0.41 ± 0.02	0.48 ± 0.01
PhO (**3a**)	517	562	569.5	7.5	0.48 ± 0.03	0.54 ± 0.03	560	568.5	8.5	0.39 ± 0.01	0.44 ± 0.01
Naphthoxy (**3b**)	517	562	570	8	0.43 ± 0.01	0.49 ± 0.01	560	568.5	8.5	0.38 ± 0.01	0.43 ± 0.01
Acetate (**4a**)	519	564	571.5	7.5	0.42 ± 0.01	0.47 ± 0.01	561.5	569.5	8	0.35 ± 0.01	0.39 ± 0.01
Benzoate (**4b**)	520	565	572	7	0.43 ± 0.01	0.47 ± 0.01	562	570	8	0.35 ± 0.01	0.37 ± 0.01
HO (**5**)	516	561	568	7	0.47 ± 0.02	0.54 ± 0.01	558	566	8	0.42 ± 0.02	0.48 ± 0.01
TMSO (**6**)	515	560	567	7	0.51 ± 0.01	0.59 ± 0.01	558	565.5	7.5	0.42 ± 0.02	0.50 ± 0.01
Ph (**7**)	522	567	573	6	0.39 ± 0.02	0.43 ± 0.01	564	571.5	7.5	0.31 ± 0.01	0.33 ± 0.01
F_5PhS (**8a**)	524	569	575	6	0.34 ± 0.01	0.38 ± 0.01	566	573.5	7.5	0.29 ± 0.01	0.32 ± 0.01
MePhS (**8b**)	521	566	573	7	0.14 ± 0.004	0.16 ± 0.003	563.5	571.5	8	0.13 ± 0.005	0.14 ± 0.004
PhMeN (**9**)	519	564	571	6	0.003 ± 4 × 10^{-4}	0.003 ± 5 × 10^{-4}	561	569.5	8.5	0.002 ± 1 × 10^{-4}	0.003 ± 1 × 10^{-4}
F_5-BsubPc (ref. 1)	—	564	570.5	6.5	0.42	—	561	569	8	—	—
PhO-F_{12}BsubPc (ref. 2)	—	572.5	579.5	7	—	0.40	567	575.5	8.5	—	—

[a] Excitation wavelength used for quantum yield measurements in toluene and α,α,α-trifluorotoluene.

spectra, with $\lambda_{max,tol}^{abs}$ of 566, 567, and 569 nm for MePhS-BsubPc (**8b**), Ph-BsubPc (**7**), and F_5PhS-BsubPc (**8a**), respectively.

The influence of the axial group on the emission spectra of BsubPcs within toluene is also minor (Fig. 3b), with the maximum emission wavelengths in toluene ($\lambda_{max,tol}^{em}$) all falling within an 8 nm range from 567–575 nm (Table 4). The slight shifts in the emission spectra of the axially substituted BsubPcs parallel the shifts seen in the absorbance spectra. F-BsubPc (**1b**), the alkoxy-BsubPcs (**2a–f**), phenoxy-BsubPcs (**3a**,**b**), HO-BsubPc (**5**), and TMSO-BsubPc (**6**) have the most blueshifted emission at $\lambda_{max,tol}^{em}$ = 567–570 nm; followed by the carboxylate-BsubPcs (**4a**,**b**), Cl-BsubPc (**1a**), and PhMeN-BsubPc (**9**) at $\lambda_{max,tol}^{em}$ = 571–572 nm; and finally Ph-BsubPc (**7**) and the thiophenoxy-BsubPcs (**8a**,**b**) at the red end of the range with $\lambda_{max,tol}^{em}$ = 573–575 nm. It is interesting to note that PhMeN-BsubPc (**9**) demonstrated almost complete fluorescence quenching, which can be seen by its jagged normalized emission spectra in both toluene (Fig. 3b) and α,α,α-trifluorotoluene (Fig. 3d).

When measured in α,α,α-trifluorotoluene, there was a general 2–3 nm blueshift in maximum absorption wavelength compared to toluene, with an even smaller blueshift seen in maximum emission wavelength (1–2 nm) (Fig. 3). The maximum absorption wavelengths of the axially substituted BsubPcs in α,α,α-trifluorotoluene $\left(\lambda_{max,F_3tol}^{abs}\right)$ are all within 8 nm, from 558–566 nm (Fig. 3c), while maximum emission wavelengths $\left(\lambda_{max,F_3tol}^{em}\right)$ are within a 7.5 nm range from 566–573.5 nm (Fig. 3d). Trends in absorbance and emission spectral shifts of the axially substituted BsubPcs in α,α,α-trifluorotoluene were identical to the shifts observed in toluene (Fig. 3, Table 4).

All investigated axially substituted BsubPcs had characteristically small Stokes shifts of 5.5–8.5 nm in both toluene and α,α,α-trifluorotoluene. The Stokes shifts in α,α,α-trifluorotoluene were 0.5–2.5 nm larger than in toluene for all investigated compounds (Table 4). The individual absorbance and emission spectra of all investigated axially substituted BsubPcs showing the slight blueshifts in the spectra from toluene to α,α,α-trifluorotoluene, along with the small Stokes shifts observed for all BsubPcs in both solvents, can be found in the ESI† (Fig. S94–S111).

Solvent polarity is one of the most important factors in determining solvatochromic effects.[56] The dielectric constant of a solvent is a measure of its polarity, with a higher dielectric constant corresponding to higher solvent polarity. α,α,α-Trifluorotoluene is more polar than toluene, with dielectric constants of 9.18 and 2.38, respectively.

The type of electronic transition can dictate whether a red- or blue-shift will result from increasing solvent polarity. If absorbance arises from a π → π* transition, increasing solvent polarity tends to result in a redshifted absorbance spectrum.[56–58] In this case, the excited state is usually more polarized than the ground state, and a polar solvent will stabilize the excited state more than it will stabilize the ground state.[57] The more polar the solvent, the better it can stabilize the excited state, therefore decreasing the energy gap between the two states.[57] This results in a lower energy transition, which is observed as a shift of λ_{max}^{abs} to a longer

wavelength (*i.e.* redshift).[57] The opposite trend is seen with n → π* transitions, with increasing solvent polarity causing a blueshift in absorbance.[56–58] In this instance, the ground state is more polarized than the excited state.[57] The lone pair interacts with the solvent such that the solvent aligns itself with the ground state to stabilize it, and when an excited state is reached, the solvent molecules don't have time to rearrange and stabilize it.[57] As a result, the ground state is more stabilized than the excited state, creating a higher energy transition that can be observed as a blueshift in the absorbance spectrum of a chromophore.[56–58] Based on these trends, it would appear that the BsubPc Q-band arises from a n → π* transition, but this is not the case. Time-dependent density-functional theory (TDDFT) calculations clearly show that the Q-band of BsubPcs arises mainly from the HOMO → LUMO π → π* transition, with only a minor contribution from the non-bonding orbitals.[59] The octupolar nature of the BsubPc aromatic system may cause slight differences in the polarity between the ground and excited states,[60,61] with the ground state polarity possibly being modestly larger than that of the excited state in this case. This could explain why blueshifts were observed with higher solvent polarity, even though the Q-band results from a π–π* transition.

Fluorescence quantum yield. Fluorescence quantum yield (QY) of the axially substituted BsubPcs was measured in toluene and α,α,α-trifluorotoluene and referenced to previously well-characterized reference standards F_5-BsubPc (0.42)[10] and PhO-F_{12}BsubPc (0.40).[8,10] Since the well-characterized quantum yield values of the reference compounds were originally measured in toluene, QY of the axially substituted BsubPcs in both toluene and α,α,α-trifluorotoluene were calculated with respect to the reference compounds in toluene. The difference in the refractive indices (n) of toluene (n = 1.496) and α,α,α-trifluorotoluene (n = 1.415) are accounted for in eqn (3).

F_5-BsubPc and PhO-F_{12}BsubPc both meet the criteria to be used as reference compounds and both have been previously used as QY reference compounds for other BsubPcs.[1,26,29,62] The degree of spectral overlap between each reference compound with three of the axially substituted BsubPcs in both toluene and α,α,α-trifluorotoluene is shown in Fig. 4. These three axially substituted BsubPcs represent the full range of absorbance and emission spectra seen for all axially substituted compounds in the array, with ButO-BsubPc (**2d**) representing the blue end of the range, benzoate-BsubPc (**4b**) representing the middle of the range, and F_5PhS-BsubPc (**8a**) representing the red end of the range. In general, F_5-BsubPc has a higher degree of spectral overlap with the axially substituted BsubPcs than PhO-F_{12}BsubPc due to the lack of peripheral functionalization of the former. Largely due to the variation in spectral overlap, QY values calculated using each of these reference compounds are not identical. The degree of variation between QY values using each of the reference compounds is therefore a point of investigation herein.

The excitation wavelength for each compound was chosen such that the emission peak could be separated from the reflectance peak, allowing for more accurate integration of the area under the emission curve.[15,63] Fluorescence spectra were recorded at several different excitation wavelengths for each compound to determine the ideal excitation wavelength. The fluorescence intensity increased as the excitation wavelength got closer to λ_{max}^{abs}, but there was no shift in the emission spectra, with the maximum emission wavelength remaining consistent *via* each excitation wavelength (Fig. 5). Furthermore, as the excitation wavelength decreased and moved further from λ_{max}^{abs}, it became easier to separate the

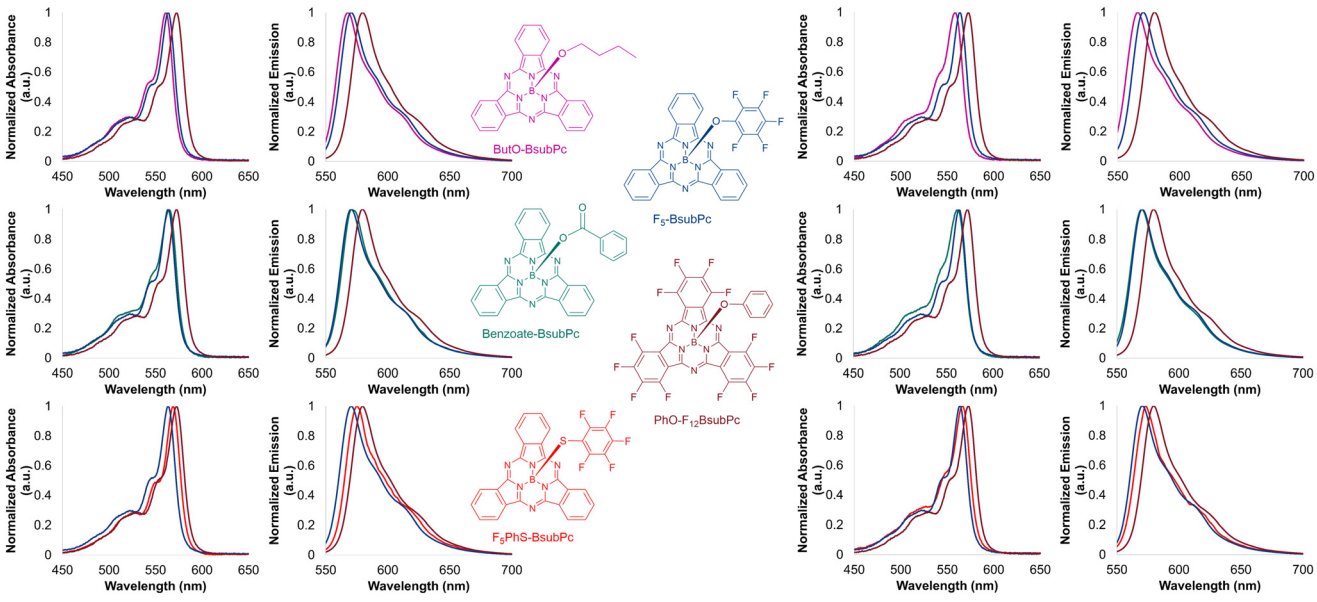

Fig. 4 Spectral overlap of F_5-BsubPc (blue) and PhO-F_{12}BsubPc (maroon) with ButO-BsubPc (top), benzoate-BsubPc (middle), and F_5PhS-BsubPc (bottom) in toluene (left) and α,α,α-trifluorotoluene (right).

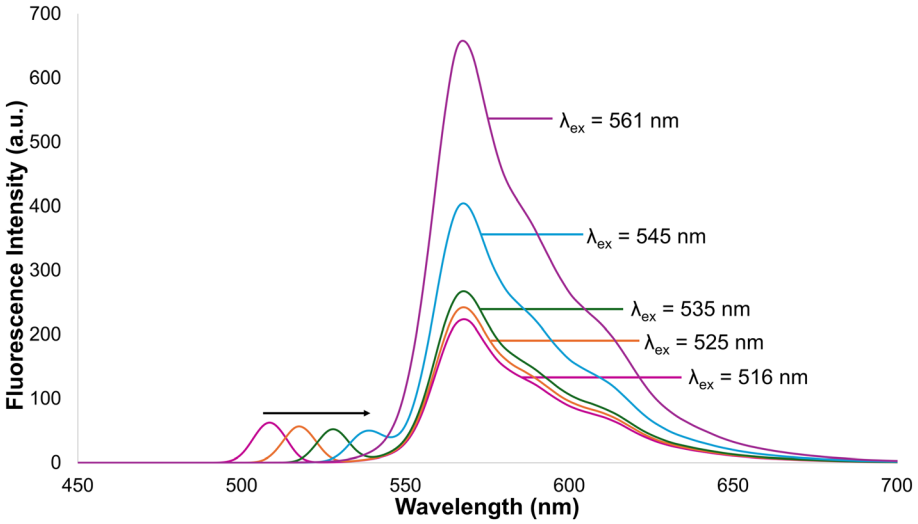

Fig. 5 Emission spectrum of butoxy-BsubPc (**2d**) in toluene with excitation wavelengths (λ_{ex}) of 516 nm (pink), 525 nm (orange), 535 nm (green), 545 nm (blue), and 561 nm (purple) and resulted in emission at 568 nm.

reflectance peak from the emission peak (Fig. 5). These observations were consistent for all axially substituted BsubPcs. An excitation wavelength that was 45 nm less than that of the maximum absorbance wavelength of each compound in toluene (eqn (2)) was used for QY measurements in both toluene and α,α,α-trifluorotoluene. While this resulted in different excitation wavelengths being used for the different BsubPcs, it allowed for a suitable excitation wavelength to be chosen for each compound with respect to its own λ_{max}^{abs}. We believe this will provide more consistent measurement conditions than choosing a single excitation wavelength that may be more suitable for some compounds than others.

The trends in QY results in toluene and α,α,α-trifluorotoluene with both reference compounds were consistent, although the actual QY values differed across the various experimental conditions: Cl-BsubPc (**1a**) had the highest QY by a significant margin, followed by F-BsubPc (**1b**) and all axial B–O bonded BsubPcs (**2**–**6**), Ph-BsubPc (**7**) with an axial B–C bond, the thiophenoxy-BsubPcs (**8a**,**b**) with axial B–S bonds, and finally PhMeN-BsubPc (**9**) with an axial B-N bond. TMSO-BsubPc (**6**), ButO-BsubPc (**2d**), and OctO-BsubPc (**2f**) were consistently on the high end of the range for B–O bonded BsubPcs, while naphthoxy-BsubPc (**3b**), acetate-BsubPc (**4a**), and benzoate-BsubPc (**4b**) were consistently on the low end. QY values were modestly higher when measured in toluene than α,α,α-trifluorotoluene, and when referenced to PhO-F_{12}BsubPc rather than F_5-BsubPc (Fig. 6, Table 4). Overall, measurements taken in toluene and referenced to PhO-F_{12}BsubPc resulted in the highest QY

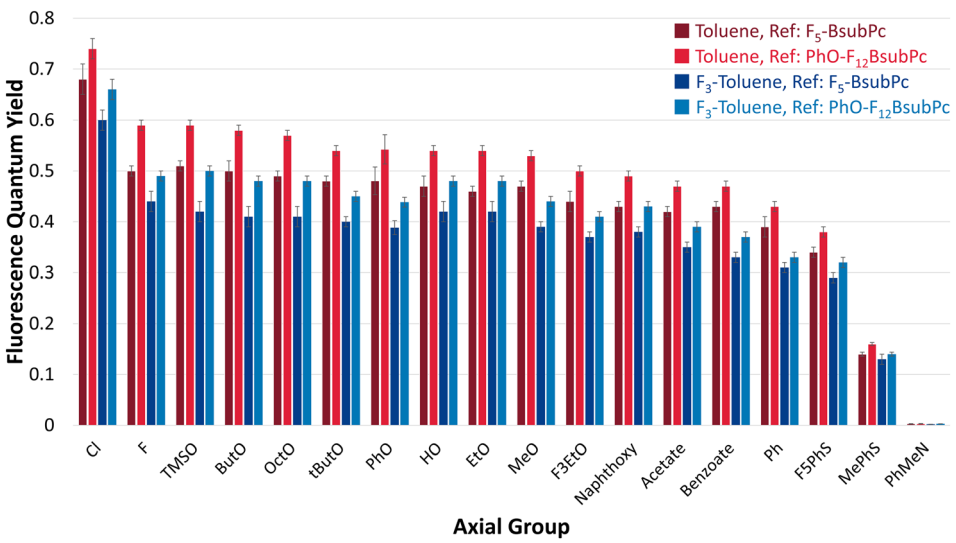

Fig. 6 Relative quantum yield of axially substituted BsubPcs measured in: toluene and referenced to F_5-BsubPc (dark red); toluene and referenced to PhO-F_{12}BsubPc (light red); α,α,α-trifluorotoluene and referenced to F_5-BsubPc (dark blue); and α,α,α-trifluorotoluene and referenced to PhO-F_{12}BsubPc (light blue).

values of the four sets of experimental conditions, followed by toluene with F_5-BsubPc, α,α,α-trifluorotoluene with PhO-F_{12}BsubPc, and α,α,α-trifluorotoluene with F_5-BsubPc (Fig. 6).

More detail, when measured in toluene and referenced to PhO-F_{12}BsubPc, the QY of Cl-BsubPc (74%) was 15% higher than the next closest compounds. The next thirteen compounds then fell within 12% of each other, with quantum yields of 47–59% for F-BsubPc and the axial B–O bonded BsubPcs. Ph-BsubPc fell just below this range with a QY of 43%. There was a significant difference in QY between the two B–S bonded BsubPcs, with F_5PhS-BsubPc (38%) having a QY 22% higher than MePhS-BsubPc (16%). Finally, PhMeN-BsubPc (**9**) showed almost complete fluorescence quenching, resulting in <1% quantum yield, which was consistent across all experimental conditions.

While still measured in toluene, there was a 2–9% decrease in QY when referenced to F_5-BsubPc compared to PhO-F_{12}BsubPc, though the trend remained the same (Table 4). While the difference in QY results was not huge when using the different reference compounds, it was large enough to have implications regarding the interpretation of results. For example, if comparing the results of F-BsubPc referenced to F_5-BsubPc with ButO-BsubPc referenced to PhO-F_{12}BsubPc, the calculation is that ButO-BsubPc has a higher QY. However, when they are referenced to the same compound, F-BsubPc and ButO-BsubPc have the same QY, and demonstrates the importance of comparing results *via* the same reference compound.

When measured in α,α,α-trifluorotoluene, there was a 2–10% decrease compared to toluene when referenced to PhO-F_{12}BsubPc, and a 3–9% decrease when referenced to F_5-BsubPc (Fig. 6, Table 4). The decrease in QY when measured in α,α,α-trifluorotoluene is aligned with the larger Stokes shift observed in α,α,α-trifluorotoluene, which indicates a higher degree of energy dissipation through non-radiative mechanisms between absorbance and emission. As seen in toluene, there was a general decrease in QY (1–8%) when referenced to PhO-F_{12}BsubPc compared to F_5-BsubPc in α,α,α-trifluorotoluene (Fig. 6, Table 4).

The almost complete fluorescence quenching displayed by PhMeN-BsubPc (**9**) under all experimental conditions can be attributed to intramolecular photoinduced electron transfer (PET), which has been observed for other BsubPcs with electron-rich axial moieties.[64,65] Aliphatic and aromatic amines (*i.e.* anilines) are also known to be fluorescence quenchers, usually through static quenching caused by the formation of a complex with the ground state of the fluorophore prior to photoexcitation.[66–69] Once excited, fluorescence quenching is caused by electron transfer from the amino group to the fluorophore.[67,68] Increased quenching is observed when there is a phenyl or methyl group on the amino group due to increased electron density, therefore enhancing the ability of the quencher to donate electrons.[68] Since PhMeN-BsubPc contains both a phenyl and a methyl group on the amino axial group, it makes sense that this BsubPc derivative is essentially non-fluorescent. The low QY of MePhS-BsubPc likely also results from intramolecular PET, with the methyl group on the axial phenyl ring contributing additional electron density.

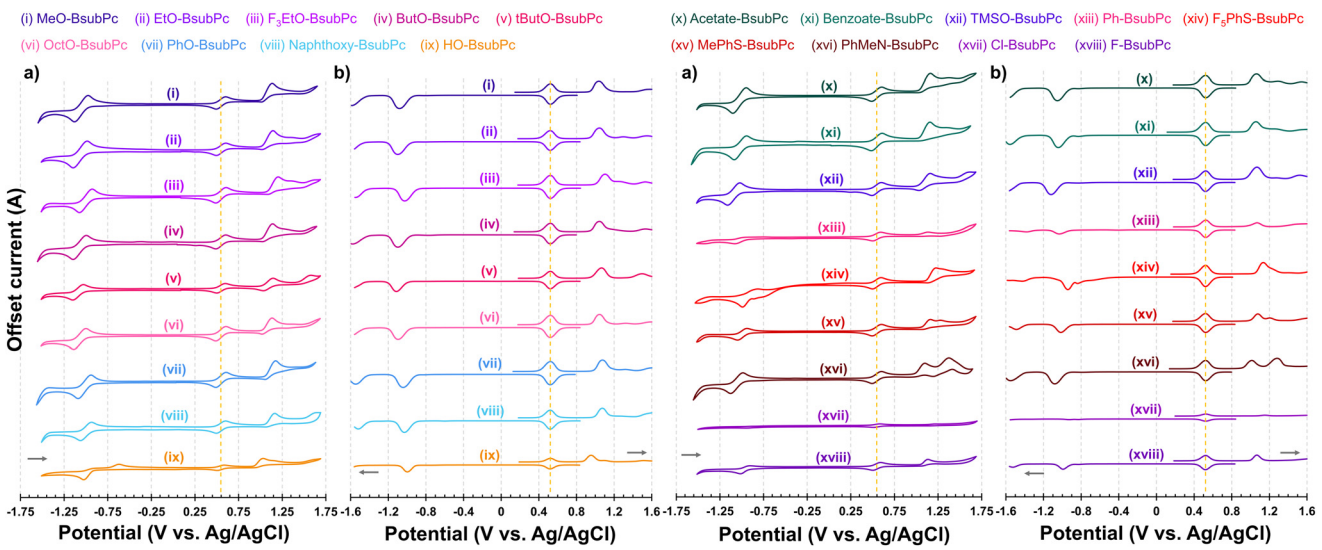

Fig. 7 a) Cyclic voltammograms and b) differential pulse voltammograms of axially substituted BsubPcs i) MeO-BsubPc, ii) EtO-BsubPc, iii) F_3EtO-BsubPc, iv) ButO-BsubPc, v) *t*ButO-BsubPc, vi) OctO-BsubPc, vii) PhO-BsubPc, viii) naphthoxy-BsubPc, ix) HO-BsubPc, x) acetate-BsubPc, xi) benzoate-BsubPc, xii) TMSO-BsubPc, xiii) Ph-BsubPc, xiv) F_5PhS-BsubPc, xv) MePhS-BsubPc, xvi) PhMeN-BsubPc, xvii) Cl-BsubPc, and xviii) F-BsubPc. Due to the low solubility of Cl-BsubPc, the peak signals cannot be clearly seen in the stacked plot, however, the peaks can be seen in the individual Cl-BsubPc CV and DPV voltammograms in the ESI† (Fig. S112). Conditions: 0.1 M tetrabutylammonium perchlorate as the electrolyte solution in nitrogen-degassed dichloromethane at room temperature with a scan rate of 100 mV s^{-1} *vs.* Ag/AgCl and ferrocene ($E_{1/2,ox}$ = 0.547 V *vs.* Ag/AgCl) as the internal reference.

Table 5 Cyclic voltammetry and differential pulse voltammetry oxidation and reduction peak (E_p) and half-wave ($E_{1/2}$) potentials of the array of axially substituted BsubPcs

	Cyclic voltammetry								Differential pulse voltammetry			
	Oxidation				Reduction				Oxidation		Reduction	
Axial group	$E^1_{1/2,ox}$ (V)	$E^1_{p,a}$ (V)	$E^2_{1/2,ox}$ (V)	$E^2_{p,a}$ (V)	$E^1_{1/2,red}$ [c] (V)	$E^1_{p,c}$ (V)	$E^2_{1/2,red}$ (V)	$E^2_{p,c}$ (V)	$E^1_{p,a}$ [f] (V)	$E^2_{p,a}$ [f] (V)	$E^1_{p,c}$ [f] (V)	$E^2_{p,c}$ [f] (V)
Cl (**1a**)	Irr	1.218[b]	—	—	Irr	−0.909[b]	—	—	1.154	—	−0.926	—
F (**1b**)	Irr	1.134[b]	—	—	−0.961	—	—	—	1.066	—	−0.994	—
MeO (**2a**)	1.073[a]	1.135[d]	—	—	−1.055	—	—	—	1.038	—	−1.082	—
EtO (**2b**)	1.081[a]	1.145	—	—	−1.066	—	—	—	1.042	—	−1.098	—
F_3EtO (**2c**)	1.143[a]	1.203[d]	—	—	−1.001	—	—	—	1.102	—	−1.026	—
ButO (**2d**)	1.083[a]	1.130[d]	—	—	−1.071	—	—	—	1.042	—	−1.098	—
*t*ButO (**2e**)	1.089[c]	1.145[e]	—	1.584[b]	−1.090	—	—	—	1.066	1.494	−1.114	—
OctO (**2f**)	1.075[a]	1.132[d]	—	—	−1.070	—	—	—	1.046	—	−1.094	—
PhO (**3a**)	1.115[a]	1.175[d]	—	—	−1.016	—	—	—	1.078	—	−1.042	—
Naphthoxy (**3b**)	1.109[a]	1.163[d]	—	—	−1.000	—	—	—	1.074	—	−1.030	—
Acetate (**4a**)	Irr	1.163[b]	—	—	−1.026	—	—	—	1.062	—	−1.054	—
Benzoate (**4b**)	Irr	1.158[b]	—	—	−1.017	—	—	—	1.058	—	−1.042	—
HO (**5**)	Irr	1.031[b]	—	—	−0.825	—	—	—	0.954	—	−0.998	—
TMSO (**6**)	1.095[a]	1.161[d]	—	1.619[b]	−1.091	—	—	—	1.070	1.522	−1.118	—
Ph (**7**)	Irr	1.133[b]	—	—	Irr	−1.080[b]	Irr	−1.433[b]	1.070	—	−1.034	−1.382
F_5PhS (**8a**)	1.175[a]	1.225[d]	—	—	Irr	−0.864[b]	−0.906[a]	−0.922[d]	1.134	—	−0.838	−0.942
MePhS (**8b**)	Irr	1.162[b]	—	—	−0.996	—	—		1.078	—	−1.014	—
PhMeN (**9**)	Irr	1.098[b]	1.290[a]	1.374[d]	−1.058	—	—		1.014	1.282	−1.082	—

[a] Quasi-reversible. [b] Irreversible. [c] Reversible. [d] Maximum peak potential from a quasi-reversible oxidation or reduction. [e] Maximum peak potential from a reversible oxidation. [f] Maximum peak potential from DPV scans.

Electrochemical characterization

CV and DPV. The CV and DPV traces for all axially substituted BsubPcs are provided in Fig. 7, and the redox potentials are summarized in Table 5. Individual CV and DPV traces of the investigated BsubPcs are provided in the ESI† (Fig. S112–S134). The CV data provided in Table 5 includes peak potentials (E_p) for irreversible redox process and half-wave potentials ($E_{1/2}$) for reversible or quasi-reversible processes. The exact half-wave potential of a quasi-reversible oxidation can be difficult to determine, so peak oxidation potentials were also reported in these cases.[26] All DPV potentials are peak potentials, as DPV does not provide information on the reversibility of a process. The typical scan range used in this study was from +1.6 V to −1.6 V, but for compounds with multiple oxidations or reductions, additional scans were run over a shorter range to evaluate the reversibility of the first oxidation/reduction.

Eighteen investigated BsubPcs displayed one reversible reduction and one to three show reversible or quasi reversible oxidation, indicating that oxidation tends to produce less stable charged species than reduction. The six compounds that displayed more unique electrochemical characteristics were Cl-BsubPc (**1a**), *t*ButO-BsubPc (**2e**), TMSO-BsubPc (**6**), Ph-BsubPc (**7**), F_5PhS-BsubPc (**8a**), and PhMeN-BsubPc (**9**). These compounds demonstrated additional redox events and/or different reversibility compared to the majority of the investigated BsubPcs.

Cl-BsubPc, Ph-BsubPc, and F_5PhS-BsubPc all had unique reduction behavior. Cl-BsubPc had an irreversible reduction at −0.909 V, along with a typical irreversible oxidation at 1.218 V, it one of the highest oxidation potentials in the array and one of the lowest reduction potentials. The quasi-reversibility of the redox events for Cl-BsubPc is consistent with previous observations.[29,62] Due to the low solubility of Cl-BsubPc, it is possible that the observed quasi-reversibility consistently results from the signal being too low for the software to pick-up (Fig. S112†).

Ph-BsubPc displayed two irreversible reductions at −1.080 V and −1.433 V, as well as an irreversible oxidation at 1.133 V (Fig. S128†). The first reduction of Ph-BsubPc was confirmed to be irreversible when a shorter scan range of +1.6 V to −1.3 V was used (Fig. S129†). The presence of two reduction peaks for Ph-BsubPc was confirmed by DPV as well.

F_5PhS-BsubPc (**8a**) also had two reductions, with an irreversible first reduction at −0.864 V and a quasi-reversible second reduction at −0.906 V. The two reductions were very close together, separated by only 42 mV (Fig. S130†). The two reduction events could be separated by running a scan in the range from +1.6 V to −1.0 V, which confirmed that the first reduction was irreversible (Fig. S131†). Therefore, the peak seen on the forward scan in the full range CV trace must result from the second reduction, meaning it is quasi-reversible. The presence of two distinct reduction events was further confirmed by DPV. Both the first and second reductions of **8a** were among the easiest reductions seen across all compounds in the array, which may be a result of the electron withdrawing fluorines in the axial group causing a slight electron deficiency of the macrocycle. This would then make reduction easier since reduction involves the gaining of electrons.

*t*ButO-BsubPc, TMSO-BsubPc, and PhMeN-BsubPc all displayed two oxidation events, along with the typical

reversible reduction. *t*ButO-BsubPc had a reversible first oxidation at 1.089 V, marking it as the only compound in the array with a fully reversible oxidation. The second oxidation at 1.584 V was irreversible (Fig. S118†). The reversibility of the first oxidation was confirmed when a shorter scan range of +1.3 V to −1.6 V was used (Fig. S119†).

The two oxidations for TMSO-BsubPc included a quasi-reversible first oxidation at 1.095 V and an irreversible second oxidation at 1.619 V (Fig. S126†). Once again, the quasi-reversible nature of the first oxidation was confirmed by an additional scan from +1.3 V to −1.6 V (Fig. S127†).

In the case of PhMeN-BsubPc, the first oxidation at 1.098 V was the irreversible one, while the second oxidation at 1.290 V was quasi-reversible (Fig. S133†). A scan from +1.2 V to −1.6 V confirmed the irreversibility of the first oxidation of PhMeN-BsubPc (Fig. S134†). The presence of two oxidation events for each of these compounds was confirmed by DPV.

TMSO-BsubPc and *t*ButO-BsubPc had the two lowest reduction potential, with half-wave potentials of −1.091 V and −1.090 V, respectively, for their reversible reductions. PhMeN-BsubPc was easier to reduce than *t*ButO- and TMSO-BsubPc with a 32–33 mV more positive half-wave reduction potential at −1.058 V. The multiple oxidation events seen for these three compounds likely result from electron donating effects from the axial group. As previously discussed in the fluorescence quantum yield section, the *N*-phenyl-*N*-methyl-amino axial group of PhMeN-BsubPc is strongly electron donating, while the electron donation from the TMSO-BsubPc axial group comes from the three methyl groups and the silicon. These results also may imply that the branched alkane of the *t*ButO-BsubPc (**2e**) axial group is more electron donating than the linear alkanes of the other five alkoxy-BsubPcs (**2a**–**d**,**f**).

Since seventeen of the eighteen compounds in this study had irreversible or quasi-reversible first oxidations, comparisons in first oxidation potential were made based on maximum peak potentials. The first oxidation potentials based on maximum peak potentials from CV spanned a 194 mV range from 1.031 V to 1.225 V. The order from lowest to highest first oxidation potential (*i.e.* from easiest to oxidize to the hardest) was based on DPV peak potentials and is a fairer comparison for compounds with varying degrees of reversibility. Furthermore, it removes the uncertainty that comes with determining half-wave potentials from quasi-reversible oxidations. The first oxidation peak potentials from DPV spanned 200 mV from 0.954 V to 1.154 V. HO-BsubPc had the lowest oxidation potential, followed by PhMeN-BsubPc, MeO-BsubPc, EtO-/ButO-BsubPc, OctO-BsubPc, benzoate-BsubPc, acetate-BsubPc, *t*ButO-/F-BsubPc, TMSO-/Ph-BsubPc, naphthoxy-BsubPc, PhO-/MePhS-BsubPc, F_3EtO-BsubPc, F_5PhS-BsubPc, and Cl-BsubPc.

An even larger range was seen for the first reduction potentials than the first oxidation potentials, spanning 266 mV from −0.825 V to −1.091 V based on CV half-wave potentials. Since three of the compounds had irreversible first reductions, comparisons were once again made based on the maximum peak potentials of the first reduction from DPV. The first reduction peak potentials from DPV spanned a 280 mV range from −0.838 V to −1.118 V. The order from easiest to reduce to most difficult to reduce based on DPV peak potentials is F_5PhS-BsubPc, Cl-BsubPc, F-BsubPc, HO-BsubPc, MePhS-BsubPc, F_3EtO-BsubPc, naphthoxy-BsubPc, Ph-BsubPc, PhO-/benzoate-BsubPc, acetate-BsubPc, MeO-/PhMeN-BsubPc, OctO-BsubPc, EtO-/ButO-BsubPc, *t*ButO-BsubPc, and TMSO-BsubPc.

Among the axial halides (**1a**,**b**), Cl-BsubPc is harder to oxidize and easier to reduce than F-BsubPc, which is in good agreement with previous reports.[1,70] Among the B–O bonded BsubPcs, the alkoxy-BsubPcs (**2a**–**f**) are generally easier to oxidize and harder to reduce than the carboxylate-BsubPcs (**4a**,**b**). This observation aligns with the carboxylate groups being electron withdrawing, while the alkoxy groups are electron donating. Similarly, F_5PhS-BsubPc (**8a**) is easier to reduce and harder to oxidize than MePhS-BsubPc (**8b**) due to the electron-withdrawing effects of the fluorines in the axial group of **8a** *versus* the electron donating effects from the axial group of **8b**.

Overall, the differences in reversibility, number of redox events, and redox potentials indicates that there is an electronic connection between the axial group and the core of the BsubPc macrocycle that influences the overall electrochemical behaviour of BsubPcs. Electron-withdrawing *versus* electron-donating effects appear to have the strongest influence, with electron-donating groups improving the reversibility and lowering the potential of oxidation processes, while electron-withdrawing groups facilitate easier reduction processes.

HOMO/LUMO estimation. The CV and DPV data described above was also used to estimate the frontier molecular orbital energy levels of the axially substituted BsubPcs. The first oxidation was used to estimate the HOMO using the equation developed by D'Andrade *et al.* (eqn (5)).[71] This equation was developed to calculate the HOMO from the half-wave potential of the first oxidation event, however, the half-wave potential is difficult to accurately determine for the compounds with quasi-reversible first oxidations and is not available for the compounds with irreversible first oxidations.[26,29] Therefore, the HOMO energy levels were estimated three times: (1) using the half-wave potential or peak potential from CV for quasi-reversible or irreversible oxidations, respectively; (2) using the peak oxidation potential from DPV; and (3) using the potential at the onset of the first oxidation peak from DPV (Table 6).[29] The calculation was done in these three ways because it is unclear which potential corresponds best with the potential modelled by eqn (5). The HOMO levels were an average of 0.13 eV deeper when estimated from the maximum peak potential from DPV compared to the onset of oxidation from DPV, and, on average, another 0.07 eV deeper when using the DPV peak potentials compared to the CV potentials (Table 6).

$$E_{\mathrm{HOMO}} = -(1.4 \pm 0.1) \times (qV_{\mathrm{CV}}) - (4.6 \pm 0.08)\ \mathrm{eV} \quad (5)$$

Table 6 HOMO, LUMO, and optical band gap estimations for the array of axially substituted BsubPcs from electrochemical characterization, UV-vis spectroscopy, and DFT modelling

	UV-vis spectroscopy		Estimated frontier orbital energies						DFT modelling	
	Toluene	α,α,α-Trifluorotoluene	CV		DPV peak		DPV onset		B3LYP 6-31G(D)	
Axial group	E_g^{opt} (eV)	E_g^{opt} (eV)	HOMO (eV)	LUMO[f] (eV)	HOMO[d] (eV)	LUMO[f] (eV)	HOMO[e] (eV)	LUMO[f] (eV)	HOMO (eV)	LUMO (eV)
Cl (**1a**)	2.14	2.17	−6.10[b]	−3.96	−6.02	−3.88	−5.91	−3.77	−5.75	−3.61
F (**1b**)	2.14	2.15	−5.99[b]	−3.85	−5.91	−3.77	−5.82	−3.68	−5.65	−3.50
MeO (**2a**)	2.14	2.15	−5.91[a]	−3.77	−5.87	−3.73	−5.74	−3.60	−5.54	−3.41
EtO (**2b**)	2.13	2.17	−5.93[a]	−3.80	−5.87	−3.74	−5.73	−3.60	−5.54	−3.39
F_3EtO (**2c**)	2.15	2.16	−6.01[a]	−3.86	−5.95	−3.80	−5.81	−3.66	−5.71	−3.57
ButO (**2d**)	2.15	2.18	−5.93[c]	−3.78	−5.87	−3.72	−5.73	−3.58	−5.55	−3.41
*t*ButO (**2e**)	2.16	2.14	−5.94[a]	−3.78	−5.91	−3.75	−5.74	−3.58	−5.51	−3.36
OctO (**2f**)	2.17	2.16	−5.92[a]	−3.75	−5.88	−3.71	−5.75	−3.58	−5.53	−3.38
PhO (**3a**)	2.15	2.15	−5.97[a]	−3.82	−5.92	−3.77	−5.78	−3.63	−5.60	−3.46
Naphthoxy (**3b**)	2.12	2.14	−5.96[a]	−3.84	−5.92	−3.80	−5.79	−3.67	−5.61	−3.48
Acetate (**4a**)	2.17	2.14	−6.03[b]	−3.86	−5.90	−3.73	−5.76	−3.59	−5.78	−3.66
Benzoate (**4b**)	2.15	2.13	−6.03[b]	−3.88	−5.90	−3.75	−5.76	−3.61	−5.57	−3.46
HO (**5**)	2.17	2.16	−5.86[b]	−3.69	−5.76	−3.59	−5.66	−3.49	−5.54	−3.41
TMSO (**6**)	2.17	2.14	−5.94[a]	−3.82	−5.91	−3.79	−5.73	−3.61	−5.54	−3.38
Ph (**7**)	2.12	2.12	−5.99[b]	−3.87	−5.91	−3.79	−5.76	−3.64	−5.55	−3.44
F_5PhS (**8a**)	2.14	2.16	−6.05[a]	−3.91	−5.99	−3.85	−5.87	−3.73	−5.81	−3.70
MePhS (**8b**)	2.12	2.13	−6.03[b]	−3.91	−5.92	−3.80	−5.80	−3.68	−5.61	−3.50
PhMeN (**9**)	2.10	2.15	−5.95[b]	−3.85	−5.84	−3.74	−5.70	−3.60	−5.51	−3.43

[a] HOMO energy level calculated using the half-wave potential from a quasi-reversible oxidation and eqn (5).[71] [b] HOMO energy level calculated using the peak oxidation potential from CV from an irreversible oxidation and eqn (5).[71] [c] HOMO energy level calculated using the half-wave potential from a reversible oxidation and eqn (5).[71] [d] HOMO energy levels calculated using the peak oxidation potential from DPV and eqn (5).[71] [e] HOMO energy levels calculated using the potential at the onset of oxidation from DPV and eqn (5).[71] [f] LUMO levels calculated by adding E_g^{opt} calculated in toluene to the estimated HOMO energy levels.

The optical band gap (E_g^{opt}) estimated from UV-vis spectroscopy was added to the estimated HOMO to calculate the LUMO. Optical band gaps were estimated from the UV-vis absorbance spectra by determining the wavelength at the intersection point between the baseline and the tangent line from where the onset of absorption occurs.[1,15,44] Band gaps were calculated for each compound in both toluene and α,α,α-trifluorotoluene using data that was acquired within this study. The axial group has a minimal impact on the band gap, which is expected due to the minor shifts in absorbance spectra. Regardless of solvent, all band gaps were within the range of 2.10–2.18 eV (Table 6). Due to the minimal difference in band gap between solvents and to be consistent with previous reports,[1,15,29] the band gaps calculated from the UV-vis spectra recorded in toluene were used in the calculation of the LUMO level.

The HOMO and LUMO levels were also estimated by DFT modelling using the B3LYP 6-31G(D) basis set and the calibration model reported by Holst *et al.* (Table 6).[72] The HOMO/LUMO energy levels calculated using the potentials from CV and the peak potentials from DPV were modestly deeper than the energy levels predicted by DFT calibration modeling and the reported values for Cl-BsubPc, F-BsubPc, and PhO-BsubPc that were HOMO-specifically measured.[29,72] It is important to note that previous electrochemical property reports did not use the exact same experimental conditions for CV and DPV as were used for this study. For example, previous reports of the HOMO/LUMO levels of Cl-BsubPc, F-BsubPc, and PhO-BsubPc used decamethylferrocene as the internal reference for CV and DPV, rather than ferrocene.[26,29] FYI – decamethylferrocene cannot be used within Canada now due to regulatory changes, therefore, ferrocene is now used. It is known that changing the internal reference may shift the correction of the redox potentials, which would also result in differences in the estimation of the frontier molecular orbital energy levels.[35]

On average, the HOMO levels estimated from the potential at the onset of oxidation from DPV were 0.16 eV deeper than the HOMO levels from DFT. By contrast, the HOMO levels were an average of 0.30 eV deeper when using the maximum peak potential from DPV compared to DFT, and 0.37 eV deeper when using CV potentials comparted to DFT. These results suggest that in the absence of a reversible first oxidation, the potential at the onset of oxidation from DPV is the best approximation for the half-wave potential when using the equation from D'Andrade *et al.* to estimate the HOMO energy level.

Conclusions

In this study, we demonstrated the utility of Br-BsubPc as an intermediate to a wide range of axial group substituents, allowing for direct axial modification with a variety of nucleophiles under relatively mild conditions. We show that high temperatures (>100 °C) and excessively long reaction times are not required for many nucleophiles, as was

previously reported to be necessary when using Cl-BsubPc as the intermediate. Furthermore, we demonstrate that compounds that were previously believed to be unattainable without the use of supplementary reagents can be formed under relatively mild conditions, therefore, reporting for the first time the synthesis of two thiophenoxy-BsubPc derivatives (**8a**,**b**) and one amino-BsubPc derivative (**9**) directly from Br-BsubPc. These results open the door for facile synthesis of a broader range of axial substituents than previously realized.

Despite the diversity of the axial groups, the UV-vis absorbance and emission spectra of the investigated BsubPcs showed minimal change, confirming that the axial group does not have a significant impact on these properties. The polarity of the solvent used in solution-state UV-vis has a minor impact on the maximum absorbance and emission of BsubPcs, with more polar solvents causing a slight blueshift. In this study, α,α,α-trifluorotoluene caused a 2–3 nm blueshift in maximum absorbance and a 1–2 nm blueshift in maximum emission compared to toluene.

The axial group had a large impact on fluorescence quantum yield (QY), with values ranging from <1% for PhMeN-BsubPc to 60–74% for Cl-BsubPc, depending on the experimental conditions. Fifteen of the eighteen compounds in the array have quantum yields between 30–60% under the various experimental conditions, which is the typical range for BsubPcs. In general, the BsubPcs with axial halides or boron–oxygen bonds had higher quantum yields than those with boron–sulfur, boron–carbon, and boron–nitrogen bonds. While the trends in QY remained constant across the various experimental conditions, the solvent and reference compound proved to have a significant enough impact to prevent direct comparisons from being made between QY values measured under different conditions.

The axial group also had a notable impact on the electrochemical properties of the BsubPcs, influencing the quantity, reversibility, and potential of the redox processes. Two-thirds of the investigated BsubPcs had one reversible reduction and one quasi-reversible or irreversible oxidation, while the remaining six compounds displayed different reversibility and/or additional redox events. First oxidation potentials based on maximum peak potentials from CV covered a 194 mV range from 1.031 V to 1.225 V, while first reduction potentials based on half-wave potentials from CV covered a 266 mV range from −0.825 V to −1.091 V. Electron-withdrawing *versus* electron-donating effects from the axial group had the largest impact on the redox behavior of the investigated array of BsubPcs.

Finally, the frontier molecular orbital energy levels were estimated in three ways from the electrochemical characterization due to the irreversible and quasi-reversible oxidations preventing the accurate determination of half-wave potentials to estimate the HOMO level. The potential at the onset of the first oxidation peak from DPV provided the best approximation for the half-wave potential to estimate the HOMO. Using this method, the HOMO levels ranged from −5.66 eV to −5.91 eV, while the calculated LUMO levels ranged from −3.49 eV to −3.77 eV.

Overall, the considerable impact of the axial group on the fluorescence quantum yield and electrochemical properties of the investigated BsubPcs shows that the axial group can be a useful synthetic tool for tuning the photophysical and electrochemical properties of BsubPcs for application in a variety of organic electronic devices. These results will help guide future materials development in the organic electronics space, providing valuable information on which axial groups to target for BsubPcs that have been functionalized around the periphery of the molecule.

Author contributions

R. Z. performed all chemical synthesis, purification, and characterization, and prepared this manuscript. This project was completed under the supervision of T. P. B.

Conflicts of interest

The authors declare no competing financial interest.

Acknowledgements

This work was supported by Mitacs through the Mitacs Accelerate program that is present within Canada. A Hatch Graduate Scholarship from Hatch Ltd (Mississauga, Ontario, Canada) regarding Sustainable Energy progress was also supportive. The authors also gratefully acknowledge the NSERC of Canada and their support of this work through a Discovery Grant (DG) to T. P. B.

References

1 N. F. Farac, A. R. Tetreault and T. P. Bender, *J. Phys. Chem. C*, 2023, **127**, 702–727.
2 B. H. Lessard and T. P. Bender, *Macromol. Rapid Commun.*, 2013, **34**, 568–573.
3 T. M. Grant, D. S. Josey, K. L. Sampson, T. Mudigonda, T. P. Bender and B. H. Lessard, *Chem. Rec.*, 2019, **19**, 1093–1112.
4 C. J. Brabec, *Sol. Energy Mater. Sol. Cells*, 2004, **83**, 273–292.
5 G. E. Morse and T. P. Bender, *ACS Appl. Mater. Interfaces*, 2012, **4**, 5055–5068.
6 H. S. Vogelbaum and G. Sauvé, *Synth. Met.*, 2017, **223**, 107–121.
7 K. Cnops, B. P. Rand, D. Cheyns, B. Verreet, M. A. Empl and P. Heremans, *Nat. Commun.*, 2014, **5**, 3406.
8 D. González-Rodríguez, T. Torres, D. M. Guldi, J. Rivera, M. Á. Herranz and L. Echegoyen, *J. Am. Chem. Soc.*, 2004, **126**, 6301–6313.
9 M. G. Helander, G. E. Morse, J. Qiu, J. S. Castrucci, T. P. Bender and Z.-H. Lu, *ACS Appl. Mater. Interfaces*, 2010, **2**, 3147–3152.
10 G. E. Morse, M. G. Helander, J. F. Maka, Z.-H. Lu and T. P. Bender, *ACS Appl. Mater. Interfaces*, 2010, **2**, 1934–1944.

11 T. G. Plint, B. H. Lessard and T. P. Bender, *Opt. Mater.*, 2018, **75**, 710–718.
12 K. Cnops, B. P. Rand, D. Cheyns and P. Heremans, *Appl. Phys. Lett.*, 2012, **101**, 143301.
13 K. Cnops, G. Zango, J. Genoe, P. Heremans, M. V. Martinez-Diaz, T. Torres and D. Cheyns, *J. Am. Chem. Soc.*, 2015, **137**, 8991–8997.
14 B. Verreet, K. Cnops, D. Cheyns, P. Heremans, A. Stesmans, G. Zango, C. G. Claessens, T. Torres and B. P. Rand, *Adv. Energy Mater.*, 2014, **4**, 1301413.
15 D. P. Holst, A. Dovijarski, A. J. Lough and T. P. Bender, *New J. Chem.*, 2021, **45**, 5791–5807.
16 C. G. Claessens, D. González-Rodríguez, M. S. Rodríguez-Morgade, A. Medina and T. Torres, *Chem. Rev.*, 2014, **114**, 2192–2277.
17 G. Lavarda, J. Labella, M. V. Martínez-Díaz, M. S. Rodríguez-Morgade, A. Osuka and T. Torres, *Chem. Soc. Rev.*, 2022, **51**, 9482–9619.
18 G. E. Morse, A. S. Paton, A. Lough and T. P. Bender, *Dalton Trans.*, 2010, **39**, 3915–3922.
19 D. S. Josey, G. L. Ingram, R. K. Garner, J. M. Wang, G. J. Evans, Z.-H. Lu and T. P. Bender, *ACS Appl. Energy Mater.*, 2019, **2**, 979–986.
20 D. S. Josey, S. R. Nyikos, R. K. Garner, A. Dovijarski, J. S. Castrucci, J. M. Wang, G. J. Evans and T. P. Bender, *ACS Energy Lett.*, 2017, **2**, 726–732.
21 G. E. Morse and T. P. Bender, *Inorg. Chem.*, 2012, **51**, 6460–6467.
22 M. Dowds and M. B. Nielsen, *Mol. Syst. Des. Eng.*, 2021, **6**, 6–24.
23 D. González-Rodríguez, T. Torres, E. L. G. Denardin, D. Samios, V. Stefani and D. S. Corrêa, *J. Organomet. Chem.*, 2009, **694**, 1617–1622.
24 C. G. Claessens, D. González-Rodríguez and T. Torres, *Chem. Rev.*, 2002, **102**, 835–854.
25 K. L. Sampson, X. Jiang, E. Bukuroshi, A. Dovijarski, H. Raboui, T. P. Bender and K. M. Kadish, *J. Phys. Chem. A*, 2018, **122**, 4414–4424.
26 K. L. Sampson, D. S. Josey, Y. Li, J. D. Virdo, Z.-H. Lu and T. P. Bender, *J. Phys. Chem. C*, 2018, **122**, 1091–1102.
27 C. G. Claessens, D. González-Rodríguez, B. del Rey, T. Torres, G. Mark, H.-P. Schuchmann, C. von Sonntag, J. G. MacDonald and R. S. Nohr, *Eur. J. Org. Chem.*, 2003, **2003**, 2547–2551.
28 G. E. Morse, J. S. Castrucci, M. G. Helander, Z.-H. Lu and T. P. Bender, *ACS Appl. Mater. Interfaces*, 2011, **3**, 3538–3544.
29 M. V. Fulford, D. Jaidka, A. S. Paton, G. E. Morse, E. R. L. Brisson, A. J. Lough and T. P. Bender, *J. Chem. Eng. Data*, 2012, **57**, 2756–2765.
30 M. Hildebrand, D. Holst, T. Bender and L. Kronik, *Adv. Theory Simul.*, 2022, **5**, 2100400.
31 E. Bukuroshi, A. U. Petersen, L. Broløs, T. P. Bender and M. B. Nielsen, *Eur. J. Inorg. Chem.*, 2020, **2020**, 3481–3495.
32 C. Würth, C. Lochmann, M. Spieles, J. Pauli, K. Hoffmann, T. Schüttrigkeit, T. Franzl and U. Resch-Genger, *Appl. Spectrosc.*, 2010, **64**, 733–741.
33 S. Fery-Forgues and D. Lavabre, *J. Chem. Educ.*, 1999, **76**, 1260.
34 C. Würth, M. Grabolle, J. Pauli, M. Spieles and U. Resch-Genger, *Nat. Protoc.*, 2013, **8**, 1535–1550.
35 E. Bukuroshi, A. Mizrahi, Z. Gross and T. P. Bender, *Eur. J. Inorg. Chem.*, 2021, **2021**, 1090–1097.
36 A. Anctil, C. W. Babbitt, R. P. Raffaelle and B. J. Landi, *Environ. Sci. Technol.*, 2011, **45**, 2353–2359.
37 A. Anctil, C. W. Babbitt, R. P. Raffaelle and B. J. Landi, *Progr. Photovolt.: Res. Appl.*, 2013, **21**, 1541–1554.
38 A. S. Paton, A. J. Lough and T. P. Bender, *Ind. Eng. Chem. Res.*, 2012, **51**, 6290–6296.
39 E. R. L. Brisson, A. S. Paton, G. E. Morse and T. P. Bender, *Ind. Eng. Chem. Res.*, 2011, **50**, 10910–10917.
40 A. S. Paton, G. E. Morse, A. J. Lough and T. P. Bender, *Cryst. Growth Des.*, 2013, **13**, 5368–5374.
41 J. D. Virdo, A. J. Lough and T. P. Bender, *Acta Crystallogr., Sect. C: Struct. Chem.*, 2016, **72**, 297–307.
42 K. A. Winterfeld, G. Lavarda, J. Guilleme, M. Sekita, D. M. Guldi, T. Torres and G. Bottari, *J. Am. Chem. Soc.*, 2017, **139**, 5520–5529.
43 P. P. Semyannikov, T. V. Basova, V. M. Grankin and I. K. Igumenov, *J. Porphyrins Phthalocyanines*, 2000, **04**, 271–277.
44 E. Bukuroshi, J. Vestfrid, Z. Gross and T. P. Bender, *New J. Chem.*, 2019, **43**, 16730–16737.
45 C. Bonnier, D. S. Josey and T. P. Bender, *Aust. J. Chem.*, 2015, **68**, 1750–1758.
46 J. Guilleme, D. González-Rodríguez and T. Torres, *Angew. Chem., Int. Ed.*, 2011, **50**, 3506–3509.
47 J. Guilleme, L. Martínez-Fernández, I. Corral, M. Yáñez, D. González-Rodríguez and T. Torres, *Org. Lett.*, 2015, **17**, 4722–4725.
48 I. Noviandri, K. N. Brown, D. S. Fleming, P. T. Gulyas, P. A. Lay, A. F. Masters and L. Phillips, *J. Phys. Chem. B*, 1999, **103**, 6713–6722.
49 C. M. A. Brett and A. M. O. Brett, *Electrochemistry: Principles, Methods, and Applications*, 1993, **https://books.google.ca/books/about/Electrochemistry.html?id=NmmeQgAACAAJ&redir_esc=y**.
50 J. D. Virdo, Y. H. Kawar, A. J. Lough and T. P. Bender, *CrystEngComm*, 2013, **15**, 3187–3199.
51 B. J. Knapik, R. Zigelstein, M. Saban and T. P. Bender, *ACS Chem. Health Saf.*, 2023, **30**(5), 287–301.
52 J. D. Dang, D. S. Josey, M. T. Dang and T. P. Bender, *ACS Omega*, 2018, **3**, 2093–2103.
53 A. S. Paton and T. P. Bender, *J. Porphyrins Phthalocyanines*, 2014, **18**, 1051–1056.
54 J. Guilleme, L. Martínez-Fernández, D. González-Rodríguez, I. Corral, M. Yáñez and T. Torres, *J. Am. Chem. Soc.*, 2014, **136**, 14289–14298.
55 C. Bonnier and T. P. Bender, *Molecules*, 2015, **20**, 18237–18245.
56 A. R., J. Hu and M. U. Momeen, *RSC Adv.*, 2023, **13**, 29489–29495.
57 A. A. Edwards and B. D. Alexander, in *Encyclopedia of Spectroscopy and Spectrometry*, ed. J. C. Lindon, G. E. Tranter and D. W. Koppenaal, Academic Press, Oxford, 3rd edn, 2017, pp. 511–519, DOI: **10.1016/B978-0-12-803224-4.00013-3**.
58 H. C. Georg, K. Coutinho and S. Canuto, *J. Chem. Phys.*, 2007, **126**, 034507.

59 A. M. Lamsabhi, M. Yáñez, O. Mó, C. Trujillo, F. Blanco, I. Alkorta, J. Elguero, E. Caballero, M. S. Rodríguez-Morgade, C. G. Claessens and T. Torres, *J. Porphyrins Phthalocyanines*, 2011, **15**, 1220–1230.
60 G. Martín, G. Rojo, F. Agulló-López, V. R. Ferro, J. M. García de la Vega, M. V. Martínez-Díaz, T. Torres, I. Ledoux and J. Zyss, *J. Phys. Chem. B*, 2002, **106**, 13139–13145.
61 C. G. Claessens, D. González-Rodríguez, T. Torres, G. Martín, F. Agulló-López, I. Ledoux, J. Zyss, V. R. Ferro and J. M. García de la Vega, *J. Phys. Chem. B*, 2005, **109**, 3800–3806.
62 E. Bukuroshi, S. Wong, T. Mudigonda, K. Nova, A. Dumont, D. Holst, Z.-H. Lu and T. P. Bender, *Mol. Syst. Des. Eng.*, 2021, **6**, 308–326.
63 D. P. Holst and T. P. Bender, *New J. Chem.*, 2021, **45**, 21082–21091.
64 C. Duan, G. Zango, M. García Iglesias, F. J. M. Colberts, M. M. Wienk, M. V. Martínez-Díaz, R. A. J. Janssen and T. Torres, *Angew. Chem., Int. Ed.*, 2017, **56**, 148–152.
65 N. Shibata, B. Das, E. Tokunaga, M. Shiro and N. Kobayashi, *Chem. – Eur. J.*, 2010, **16**, 7554–7562.
66 S. Bakkialakshmi, P. Selvarani and S. Chenthamarai, *Spectrochim. Acta, Part A*, 2013, **105**, 557–562.
67 J. R. Lakowicz, in *Principles of Fluorescence Spectroscopy*, ed. J. R. Lakowicz, Springer US, Boston, MA, 2006, ch. 8, pp. 277–330, DOI: **10.1007/978-0-387-46312-4_8**.
68 J. R. Lakowicz, in *Principles of Fluorescence Spectroscopy*, ed. J. R. Lakowicz, Springer US, Boston, MA, 2006, ch. 9, pp. 331–351, DOI: **10.1007/978-0-387-46312-4_9**.
69 D. Nagaraja, R. M. Melavanki and N. R. Patil, *Can. J. Phys.*, 2013, **91**, 966–970.
70 A. Mizrahi, E. Bukuroshi, J. Vestfrid, T. P. Bender and Z. Gross, *Inorg. Chem.*, 2020, **59**, 2641–2645.
71 B. W. D'Andrade, S. Datta, S. R. Forrest, P. Djurovich, E. Polikarpov and M. E. Thompson, *Org. Electron.*, 2005, **6**, 11–20.
72 D. P. Holst, P. Friederich, A. Aspuru-Guzik and T. P. Bender, *J. Chem. Inf. Model.*, 2022, **62**, 829–840.